

### Public Domain Mark 1.0 Universal

This work was written as part of one of the author's official duties as an Employee of the United States Government and is therefore a work of the United States Government. In accordance with 17 U.S.C. 105, no copyright protection is available for such works under U.S. Law.

Access to this work was provided by the University of Maryland, Baltimore County (UMBC) ScholarWorks@UMBC digital repository on the Maryland Shared Open Access (MD-SOAR) platform.

### **Please provide feedback**

Please support the ScholarWorks@UMBC repository by emailing [scholarworks-group@umbc.edu](mailto:scholarworks-group@umbc.edu) and telling us what having access to this work means to you and why it's important to you. Thank you.



## Regional mapping of gross light-use efficiency using MODIS spectral indices

G.G. Drolet<sup>a</sup>, E.M. Middleton<sup>b</sup>, K.F. Huemmrich<sup>b,c</sup>, F.G. Hall<sup>b,c</sup>, B.D. Amiro<sup>d</sup>, A.G. Barr<sup>e</sup>,  
T.A. Black<sup>f</sup>, J.H. McCaughey<sup>g</sup>, H.A. Margolis<sup>a,b,\*</sup>

<sup>a</sup> Centre d'Étude de la Forêt, Faculté de Foresterie et de Géomatique, Université Laval, Sainte-Foy, Québec, Canada G1K 7P4

<sup>b</sup> Biospheric Sciences Branch, Code 614.4, NASA/Goddard Space Flight Center, Greenbelt, MD 20771, USA

<sup>c</sup> Joint Center for Earth Systems Technology, University of Maryland, Baltimore County, Baltimore, MD 21228, USA

<sup>d</sup> Department of Soil Science, University of Manitoba, Winnipeg, Manitoba, Canada R3T 2N2

<sup>e</sup> Atmospheric Sciences and Technology Directorate, Meteorological Service of Canada, Saskatoon, Saskatchewan, Canada S7N 3H5

<sup>f</sup> Faculty of Agricultural Sciences, University of British Columbia, Vancouver, British Columbia, Canada V6T 1Z4

<sup>g</sup> Department of Geography, Queen's University, Kingston, Ontario, Canada K7L 3N6

### ARTICLE INFO

#### Article history:

Received 2 November 2007

Received in revised form 27 February 2008

Accepted 1 March 2008

#### Keywords:

Photochemical Reflectance Index

Gross light-use efficiency

MODIS

Flux towers

Gross ecosystem productivity

Boreal forest

Regional mapping

Shadow fraction

### ABSTRACT

Direct estimation of photosynthetic light-use efficiency (LUE) from space would be of significant benefit to LUE-based models which use inputs from remote sensing to estimate terrestrial productivity. The Photochemical Reflectance Index (PRI) has shown promise in tracking LUE at the leaf- to small canopy levels, but its use at regional to global scales still remains a challenge. In this study, we used different formulations of PRI calculated from the MODIS ocean band centered at 531 nm and a set of alternative reference bands at 488, 551, and 678 nm to explore the relationship between PRI and LUE where LUE was measured at eight eddy covariance flux towers located in the boreal forest of Saskatchewan, Canada. The magnitude and variability of LUE was significantly lower at the times when useful MODIS ocean band images were available (i.e. around midday under clear-sky conditions) relative to the rest of the growing season. PRI<sub>678</sub> (reference band at 678 nm) showed the strongest relationship ( $r^2=0.70$ ) with LUE<sub>90a</sub> (i.e. 90-minute mean LUE calculated using Absorbed Photosynthetically Active Radiation, APAR), but only when all sites were combined. Overall, the relationships between the MODIS PRIs and LUE<sub>90a</sub> were always stronger for observations closer to the backscatter direction and there were no significant differences in the strength of the correlations whether LUE was calculated based on incident PAR or on APAR. Predictions of ecosystem photosynthesis at the time of the MODIS overpasses were significantly improved by multiplying either PAR or APAR by MODIS PRI ( $r^2$  improved from 0.09 to 0.44 and 0.54 depending on the PRI formulation). We used our PRI-LUE model to create a regional LUE<sub>90a</sub> map for the three cover types covering 47,500 km<sup>2</sup> around the flux sites. The MODIS PRI-derived LUE<sub>90a</sub> map appeared to capture more realistic spatial heterogeneity of LUE across the landscape compared to a daily LUE map derived using the look-up table in the MODIS GPP (MOD17) algorithm. While our LUE map is only a snapshot of minimum regional LUE<sub>90a</sub> values, with appropriate gap-filling methods it could be used to improve regional-scale monitoring of GPP. Moreover, the strong relationship between midday and daily LUE on clear days ( $r^2=0.93$ ) indicates that instantaneous MODIS observations of LUE<sub>90a</sub> could be used to estimate daily LUE. Finally, pixel shadow fraction from the 5-Scale geometric-optical model was closely related to both MODIS PRI and tower-derived LUE suggesting that differences in stand leaf area and in diffuse illumination among flux sites play a role in the relationship we observed between LUE and MODIS PRI.

© 2008 Elsevier Inc. All rights reserved.

### 1. Introduction

Ecosystem process models coupled with inputs derived from remotely sensed data are among the most powerful tools for monitoring the temporal and spatial variations in vegetation produc-

tivity at regional to global scales (Running et al., 1999; Turner et al., 2004a,b). This approach is used in several models to estimate ecosystem photosynthesis and/or Net Primary Productivity (NPP) (e.g., Liu et al., 1997; Potter et al., 1993; Prince & Goward, 1995; Running et al., 1989). When ecosystem photosynthesis is calculated via an ecosystem process model, we refer to it as Gross Primary Productivity (GPP). On the other hand, when it is calculated from flux tower data (see below), we refer to it as Gross Ecosystem Productivity (GEP). Ecosystem models vary in their complexity and in the number of parameters and input variables, ranging from simple light-use

\* Corresponding author. Centre d'Étude de la Forêt, Faculté de Foresterie et de Géomatique, Université Laval, Sainte-Foy, Québec, Canada G1K 7P4. Tel.: +1 418 656 7120; fax: +1 418 656 5262.

E-mail address: [hank.margolis@sbf.ulaval.ca](mailto:hank.margolis@sbf.ulaval.ca) (H.A. Margolis).

efficiency (LUE) models (Potter et al., 1993; Ruimy et al., 1994) to highly sophisticated mathematical models operating at finer spatial (leaf to canopy) and temporal (hours to weeks) scales such as ECOSYS (Grant & Nalder, 2000) or BIOMASS (McMurtrie et al., 1990).

The LUE model was initially developed from the linear relationship that exists between the amount of photosynthetically active radiation (PAR) absorbed by vegetated canopies (APAR), and their net or gross primary productivity (Monteith, 1972). The efficiency with which plants use solar energy to assimilate carbon is represented in this model by a conversion factor ( $\text{mol CO}_2 \text{ mol}^{-1}$  photons absorbed or  $\text{g C MJ}^{-1}$ ), referred to as LUE for both GPP (gross LUE,  $\epsilon_g$ ) and for NPP (net LUE,  $\epsilon_n$ ).

LUE differs across biomes, plant functional types, stages of succession, and species (Gower et al., 1999), and is also temporally dynamic in response to environmental variations (Landsberg & Waring, 1997; Nouvellon et al., 2000; Turner et al., 2003). Because of this intrinsic variability, obtaining reliable LUE estimates remains a challenging task. Currently, the MOD17 algorithm (Heinsch et al., 2003; Martel et al., 2005; Running et al., 2004; Zhao et al., 2005) combines inputs from the MODerate Resolution Imaging Spectroradiometer (MODIS) onboard the Terra and Aqua satellites with meteorological data from the NASA Goddard Space Flight Center Global Modeling and Assimilation Office (GMAO) to produce global fields of daily GPP at the 1-km spatial resolution. In the MOD17 GPP algorithm, the LUE term is a maximum biome-specific ( $\epsilon_{\text{max}}$ ) value retrieved for each pixel from a biome parameter look-up table (BPLUT). Subsequently,  $\epsilon_{\text{max}}$  is scaled down using environmental variables from the GMAO, in an attempt to represent the physiological status of the vegetation at a given point in time. The BPLUT approach to estimating pixel-level LUE was identified as a source of error in MOD17 GPP estimates (Martel et al., 2005; Schwalm et al., 2006), and potential avenues for refining this method were suggested, such as calibration of gross LUE based on flux tower observations (Turner et al., 2003; Heinsch et al., 2006). Clearly, GPP estimates such as those from the MOD17 algorithm would greatly benefit from the capability to estimate gross LUE directly from space-based remote sensing.

Currently, eddy covariance (EC) flux towers are the most direct means to obtain near real-time canopy-level gross LUE estimates at high frequencies (half-hour) and over extended periods of time (years to decades). EC towers measure the exchange of trace gases ( $\text{CO}_2$ ,  $\text{CH}_4$ , etc.), water vapor, and energy between an ecosystem (encompassed within a flux footprint generally ranging between 0.5 and one  $\text{km}^2$ ) and the atmosphere (e.g., Baldocchi & Vogel, 1996; Black et al., 1996; Goulden et al., 1996; Margolis et al., 2006; Wofsy et al., 1993). Simultaneously, measurements of key variables, such as air temperature, radiation, relative humidity, soil temperature, and soil moisture are generally also made at the flux sites to aid in interpreting the flux data. However, while they provide a rich sampling of the temporal space, EC-derived gross LUE estimates represent only a relatively small fraction of the landscape and are therefore not very useful for scaling-up directly to regional and global levels.

Over the last fifteen years, much progress has been made toward using spectral indices to remotely track changes in plant physiological status (e.g., Filella et al., 1996; Fuentes et al., 2006; Gamon et al., 1997; Hill et al., 2006; Rahman et al., 2004; Serrano & Penuelas, 2005; Sims et al., 2006). Along with solar-induced fluorescence, the Photochemical Reflectance Index (PRI) (Gamon et al., 1992) appears to be one of the most promising approaches for directly estimating LUE from leaf reflectance (Grace et al., 2007).

The PRI is based on a photoprotective mechanism involving xanthophyll cycle pigments (Bilger & Björkman, 1990; Demmig-Adams, 2003). Under excessive irradiance conditions, violaxanthin pigments are de-epoxidized into antheraxanthin and zeaxanthin to avoid irreversible damage to the photosynthetic apparatus (Yamamoto, 1979). In addition to dissipating harmful extra energy as heat, this rearrangement of the pigments gives rise to a change in the

reflectance of leaves at 531 nm (Gamon et al., 1990). The PRI uses the reflectance in a narrow band ( $\approx 2\text{--}10 \text{ nm}$ ) centered at 531 nm and a reference band (generally at 570 nm). Since the de-epoxidation of the xanthophyll pigments is a trade-off between protection of the photosystems and photosynthetic efficiency, it is possible to relate the PRI to corresponding changes in photosynthetic LUE (e.g., Filella et al., 1996; Penuelas et al., 1995). While in general the correlations between the PRI and LUE are strong at the leaf- to small canopy levels, use of the relationship over larger regions has proven more difficult.

The MODIS sensor was not originally planned for PRI studies but it has several 10 nm-wide bands designed for ocean remote sensing which are suitable for calculating PRI. Most importantly, MODIS has a band centered at 531 nm (band 11) with the potential for detecting reflectance changes associated with xanthophyll cycle pigments. Rahman et al. (2004) and Drolet et al. (2005) found a relationship between a MODIS-derived PRI and LUE estimates from EC towers for temperate and boreal deciduous forests, respectively. Drolet et al. (2005), however, found a PRI:LUE relationship only for those MODIS images acquired close to the backscattering direction, suggesting possible effects due to changes in canopy shadow fraction. As well, the PRI:LUE relationship detected by Drolet et al. (2005) was stronger when using top-of-atmosphere than at-surface reflectance data to calculate the PRI, suggesting an influence of atmospheric aerosols on this relationship (Barton & North, 2001).

Several difficulties arise in interpreting measurements of PRI at the 1-km resolution of a MODIS pixel. These include the interference from variations in the concentration of other pigments such as chlorophyll and carotenoids, differences in view and illumination conditions, effects of canopy structure on spectral reflectance, and accuracy of atmospheric correction (Barton & North, 2001; Grace et al., 2007). Even though MODIS is not perfectly suited to PRI studies (e.g., lack of a reference band at 570 nm, coarse spatial resolution, midday overpass time), its daily global coverage, geolocation accuracy and high spectral resolution make it an appropriate choice for exploring the PRI:LUE relationship at the regional scale and for investigating the relationship between PRI, gross LUE, and shadow fraction. In this study, we examine (1) the inter- and intra-annual variability in midday gross LUE derived using data from eight boreal flux sites in Saskatchewan, Canada; (2) the differences in LUE across the sites and cover types; and (3) the correlation between tower-based gross LUE and a suite of MODIS-derived PRIs calculated using alternative reference bands. Using the results found in (1), (2), and (3), we create a regional map of gross LUE and compare it to a LUE map derived using the MOD17 approach. Finally, we investigate the effect of shadow fraction on the relationship between LUE and PRI.

## 2. Methods

### 2.1. Study sites

This study focuses on a region in central Saskatchewan near the southern boundary of the boreal forest. Within the study area, there are a cluster of eight eddy covariance towers. This area was chosen because (1) the cluster encompasses the major cover types found in the Canadian boreal zone, (2) there are two chronosequences representing the two major types of disturbance (timber harvesting and wildfires) that affect large areas of the Canadian boreal forest, and (3) multi-year datasets of  $\text{CO}_2$  fluxes and meteorological variables are available at most of the sites for the period covered by MODIS. These flux sites were all part of the Fluxnet-Canada Research Network (FCRN; Margolis et al., 2006), now transformed into the Canadian Carbon Program. These research networks study the impact of climate and disturbance on the productivity of forests and wetlands across Canada (<http://www.fluxnet-canada.ca>).

This specific cluster of flux towers is operated and maintained by the Boreal Ecosystem Research and Monitoring Study (BERMS) led by

**Table 1**  
Summary of site characteristics

| Site <sup>a</sup> | MODIS <sup>b</sup><br>land<br>cover | Origin <sup>c</sup> | Latitude<br>(° N) | Longitude<br>(° W) | Age<br>(years) | Height<br>(m)                     | Density<br>(stems/ha) | Overstory  | Understory and ground cover  | LAI <sup>d</sup><br>(m/m) | References                 |
|-------------------|-------------------------------------|---------------------|-------------------|--------------------|----------------|-----------------------------------|-----------------------|--|--|---------------------------|----------------------------|
| SOBS              | ENF                                 | F–N                 | 53.987            | 105.118            | 125            | 7.2                               | ~6000                 | <i>Picea mariana</i>   | <i>Pleurozium</i> spp., <i>Spagnum</i> spp.,<br>lichens, low shrubs  | 5.6                       | Jarvis et al.<br>(1997)    |
| OJP               | ENF                                 | F–N                 | 53.916            | 104.692            | 90             | 15.7                              | ~1875                 | <i>Pinus banksiana</i>   | Alder ( <i>Alnus crispa</i> ), <i>Ledum</i><br><i>groenlandicum</i> , lichens  | 3.4                       | Baldocchi<br>et al. (1997) |
| HJP75             | ENF                                 | H–N                 | 53.876            | 104.645            | 30             | 6.3                               | ~8000                 | <i>P. banksiana</i>  | <i>A. crispa</i> , lichens, grasses, fallen logs.  | 4.3                       | FCRN-DIS                   |
| HJP94             | ENF                                 | H–P                 | 53.908            | 104.656            | 13             | 1–2.6                             | ~6000                 | <i>P. banksiana</i>  | Grasses, shrubs, woody debris,<br>bare soil  | 0.6–1.0                   | Amiro et al.<br>(2006)     |
| HJP02             | MF                                  | H–P                 | 53.945            | 104.649            | 5              | ~0.1                              | –                     | –  | <i>P. banksiana</i> , lichens, grasses,<br>woody debris, bare soil   | 1.3                       | FCDN-DIS                   |
| F77               | ENF                                 | F                   | 54.485            | 105.817            | 30             | 7.4                               | ~10,500               | <i>P. banksiana</i> <i>P. mariana</i>  | <i>P. mariana</i> , <i>Vaccinium myrtilloides</i> ,<br><i>Cornus canadensis</i> , <i>Ledum groenlandicum</i>   | 2.9                       | Amiro et al.<br>(2006)     |
| F89               | MF                                  | F                   | 54.254            | 105.877            | 18             | 5                                 | ~3700                 | <i>P. banksiana</i> , <i>P. mariana</i> ,<br><i>Populus tremuloides</i>        | <i>P. mariana</i> , <i>A. crispa</i> , <i>Rosa acicularis</i> ,<br><i>Rubus idaeus</i> , <i>V. myrtilloides</i> ,<br><i>C. canadensis</i> , grasses  | 3.0                       | Amiro et al.<br>(2006)     |
| F98               | Oshrub                              | F                   | 54.091            | 106.005            | 9              | Standing<br>dead: 20<br>Live: 1–2 | ~1000<br>~50,000      | Living trees: <i>P. banksiana</i><br><i>P. mariana</i> , <i>P. tremuloides</i> | <i>Epilobium angustifolium</i> , <i>Carex</i> spp.,<br><i>V. myrtilloides</i> , <i>Rubus idaeus</i> ,<br><i>Marchantia</i> spp., coarse woody debris | 1.0                       | Amiro et al.<br>(2006)     |

<sup>a</sup> Site names: SOBS, old black spruce, OJP, old jack pine, HJP75, harvested jack pine 1975, HJP94, harvested jack pine 1994, HJP02, harvested jack pine 2002, F77, fire 1977, F89, fire 1989, F98, fire 1998.

<sup>b</sup> MODIS biome-level land cover types: ENF, evergreen needleleaf forest; MF, mixed forest, and Oshrub, open shrublands.

<sup>c</sup> F: fire; H: harvest; N: regenerated naturally after disturbance; P: planted shortly after disturbance.

<sup>d</sup> LAI values reported in this table come from different measurement techniques which are reported in Schwalm et al. (2006). They represent the total of overstory and understory LAI.

Environment Canada. A summary of key attributes of the flux sites is presented in Table 1, along with references to articles containing more detailed site descriptions. As well, additional descriptions of the site characteristics can be found in Coursolle et al. (2006) and Schwalm et al. (2006).

## 2.2. MODIS data

### 2.2.1. Surface reflectance

Terra- and Aqua-MODIS at-sensor radiance data (MOD02/MYD02, Collection 4) at 1 km spatial resolution coincident with flux tower measurements were acquired over the study sites for the clear days of the growing seasons between 2001 and 2004. Clear days were identified using time-series of downwelling PAR measured by the tower instruments. Only days which had nearly perfect diurnal PAR curves indicating no clouds were chosen. The images acquired for those days were georeferenced to a linear projection using the HDFLook software version 7, and visually inspected to eliminate potential risks of cloud contamination from neighboring pixels.

For this study, a growing season was defined as the period between June 1 (day 152) and August 31 (day 243) to minimize potential variations in stand structural properties (e.g., phenology, snow) that can occur between MODIS images distributed over a whole year. For each MODIS acquisition, the top-of-atmosphere (TOA) radiance in bands 1 (645 nm), 2 (858.5 nm), 10 (488 nm), 11 (531 nm), 12 (551 nm), 13 (667 nm), and 14 (678 nm), and view and illumination geometry (MOD03/MYD03, Collection 4) were extracted for the 1-km pixel closest to each flux tower (referred to as the “tower pixel” in this study). Bands 1 and 2 have bandwidths of 50-nm and 35-nm, respectively, and have ground instantaneous field of views (GIFOVs) of 250 m. Bands 10 to 14 are 10-nm-wide bands that were originally designed for ocean biological studies with nadir GIFOVs of 1 km, but are spectrally well-suited for PRI studies (Drolet et al., 2005).

All acquisitions with a view zenith angle larger than 45° at the center of the image were rejected to reduce possible noise associated with spatial integration of the radiance signal over large areas. TOA radiances were converted to TOA reflectances and processed using the 6S model (Vermote et al., 1997), along with concomitant aerosol optical thickness values (AOT) derived from MODIS data (MOD04/MYD04, Collection 4) to obtain surface reflectance for each clear

observation of a flux tower since this is the most relevant measure of reflectance for PRI studies. For cases where no AOT value was available over a tower, AOT values in a 9-by-9 pixel window around the tower pixel were averaged and used in 6S. In cases where no AOT value was available in the 9-by-9 pixel window, the observation was rejected from the dataset. No BRDF corrections were applied to normalize the surface reflectance data to reference view/illumination conditions. In total, 99 MODIS observations of the study sites were used in this study. Details about the MODIS observations used (e.g., time of acquisition, view/sun zenith angles, distance from tower) are available upon request to the corresponding author.

### 2.2.2. Photochemical Reflectance Index (PRI) and NDVI

MODIS surface reflectances ( $\rho_\lambda$ ) were used to calculate four different formulations of the PRI using different reference bands, and the Normalized-Difference Vegetation Index (NDVI), as a comparison to the PRIs (Eqs. (1) and (2)).

$$PRI_{\lambda\text{reference}} = (\rho_{531\text{ nm}} - \rho_{\lambda\text{ref}}) / (\rho_{531\text{ nm}} + \rho_{\lambda\text{ref}}) \quad (1)$$

$$NDVI = (\rho_{858.5\text{ nm}} - \rho_{645}) / (\rho_{858.5\text{ nm}} + \rho_{645}). \quad (2)$$

In Eqs. (1) and (2),  $\rho$  represents the surface reflectance of a MODIS band with the subscript referring to the wavelength of the band center. In Eq. (1),  $\rho_{531\text{ nm}}$  represents MODIS reflectance in band 11 (531 nm), which is the detection band containing the xanthophyll signal (Gamon et al., 1990), whereas  $\lambda_{\text{ref}}$  represents the wavelength of the band used as the reference band in the PRI. In theory, this reference band should not be affected by variations in xanthophyll cycle pigments. Unfortunately, MODIS lacks a narrow band at 570 nm, the wavelength that has generally been used as the reference wavelength in the PRI (e.g., Gamon et al., 1992; Nichol et al., 2000; Rahman et al., 2001; Styliniski et al., 2002). As surrogate reference bands, we tested alternative wavebands available from the MODIS sensor, i.e., 488 nm, 551 nm, 667 nm, and 678 nm.

### 2.2.3. $f_{\text{APAR}}$

For the calculation of APAR in the LUE term to be described in Section 2.3.1, we downloaded time-series of 8-day composites of the fraction of absorbed PAR ( $f_{\text{APAR}}$ ) derived from the MODIS-Terra



**Table 2**  
MOD15  $f_{APAR}$  values from MODIS-based measurements at the BERMS flux sites

| Site  | Mean MOD15 $f_{APAR}$ <sup>a</sup> | Mean MOD15 $f_{APAR}$ for overpass days used in the LUE analysis <sup>b</sup> | Range <sup>c</sup> |
|-------|------------------------------------|---|--------------------|
| SOBS  | 0.85                               | 0.82  | 0.79–0.90          |
| OJP   | 0.81                               | 0.81  | 0.70–0.88          |
| HJP75 | 0.84                               | 0.88  | 0.79–0.88          |
| HJP94 | 0.81                               | 0.86  | 0.71–0.89          |
| HJP02 | 0.60                               | 0.65  | 0.55–0.65          |
| F77   | 0.89                               | 0.89  | 0.87–0.93          |
| F89   | 0.92                               | 0.92  | 0.89–0.93          |
| F98   | 0.75                               | 0.81  | 0.40–0.88          |

<sup>a</sup> Mean of all growing season MODIS MOD15  $f_{APAR}$  values (Collection 4) for each tower pixel when MOD15 values were flagged as excellent quality. A growing season is defined as the days between 152 (June 1) and 243 (August 31).

<sup>b</sup> Mean of all MODIS MOD15  $f_{APAR}$  values (Collection 4) that were flagged as excellent quality for which tower flux data and MODIS reflectance data required for calculating PRI were also available.

<sup>c</sup> Range (min–max) of MODIS MOD15  $f_{APAR}$  values shown in previous column.

instrument (MOD15, Collection 4). For each clear MODIS observation over a flux tower, the eight-day  $f_{APAR}$  value on the closest date to that of the observation, and which was also flagged as “excellent quality”, was used in the calculation of APAR. Recent validation studies showed that the MODIS  $f_{APAR}$  can overestimate (e.g., Cheng et al., 2006; Steinberg et al., 2006) canopy-level  $f_{APAR}$  relative to tower or ground based measurements, notably in more open cover types. For example, Fensholt et al. (2004) found an 8–20% overestimation in the MODIS  $f_{APAR}$  of an African semi-arid shrubland. The goal of our study is to evaluate the potential for developing a new GPP algorithm that replaces the LUE adjustments in the MODIS GPP algorithm with LUE values estimated from PRI. Therefore, it was highly desirable to use the same types of input in the development of the new algorithm as that used in the current algorithm. Any errors in the  $f_{APAR}$  values are noise that we expect to have when we implement this new algorithm. Note that we would not want to use more accurate  $f_{APAR}$  values even if they were available for the overpasses during the four-year period of data collection in the current study because they could give a false impression of the potential usefulness of the new algorithm in comparison to the current MODIS GPP algorithm. The MODIS  $f_{APAR}$  values for the study sites are shown in Table 2 and details about the MODIS  $f_{APAR}$  algorithm and related pertinent information can be found in Lotsch et al. (2003), Myneni et al. (1997), and Yang et al. (2006). Note that  $f_{APAR}$  is not an inherent property of the vegetation but rather varies diurnally and seasonally with changes in sun angles, radiation conditions, and phenology. However, radiative transfer models show that changes in  $f_{APAR}$  should be small within the space of a few hours near solar noon under clear-sky conditions (Chen, 1996; Myneni et al., 1997).

#### 2.2.4. Land cover classification

To determine what biome-level cover type was assigned by the MODIS Global Land Cover Type product (MOD12Q1) at the locations of our flux towers, we downloaded MOD12Q1 (Collection 4) and used the same cover type classification scheme as for the MODIS GPP algorithm (University of Maryland cover type classes – UMD). There were three different biome cover types for our study sites: (1) evergreen needleleaf forests (ENF), (2) mixed forests (MF), and (3) open shrublands (Oshrub). Since we wanted to compare our estimates of LUE to the LUE values that would be used in the MOD17 approach to modeling GPP, we did not change the MOD12Q1 cover types assigned to each study area, even though we found misclassifications in the MODIS product at some sites.

#### 2.3. Flux and meteorology data

From the FCRN Data Information System, we downloaded for each site all available time-series of 30-minute net ecosystem productivity (NEP) and PAR for the growing seasons from 2001 through 2004

(Table 3). For the calculation of GEP, we also downloaded meteorological variables such as air and soil temperatures that were needed by the standard FCRN GEP algorithm (see appendices in Barr et al., 2004, and in Amiro et al., 2006). Using this algorithm, we produced gap-filled, 30-minute time-series of growing season GEP and downwelling PAR (GEP<sub>30</sub> and PAR<sub>30</sub>, respectively).

##### 2.3.1. Gross light-use efficiency

For each site, time-series of 30-minute gross LUE were calculated using the GEP<sub>30</sub> and PAR<sub>30</sub> time-series. Note that in further calculations of LUE, the subscripts “30” and “90” refer to either 30- or 90-minute periods centered around the MODIS overpass time, respectively; the subscripts “a” and “i” refer to LUE calculated using either absorbed or incident PAR, respectively. From a physiological standpoint, LUE is related more closely to APAR than incoming PAR. However, since reliable and consistent time-series of  $f_{APAR}$  are difficult to obtain and validate, LUE was calculated in two ways and the results obtained from the two methods were compared. With the first method, LUE<sub>30i</sub> was calculated as the ratio of GEP<sub>30</sub> to incident PAR<sub>30</sub>.

$$LUE_{30i} = GEP_{30} / PAR_{30}. \quad (3)$$

This produced estimates based solely on tower-based measurements for both GEP and PAR. To reduce the inherent variability associated with flux measurements made using the EC technique, GEP<sub>30</sub> and PAR<sub>30</sub> data coincident with MODIS overpasses were averaged to 90-minute periods. This was achieved by calculating the mean of three consecutive GEP<sub>30</sub> or PAR<sub>30</sub> values centered on the periods encompassing clear MODIS observations. LUE<sub>90i</sub> was then calculated using Eq. (3) with the 90-minute average GEP (GEP<sub>90</sub>) and PAR (PAR<sub>90</sub>) replacing GEP<sub>30</sub> and PAR<sub>30</sub>. The second method produced LUE<sub>30a</sub> calculated as GEP<sub>30</sub> divided by APAR. In this case, APAR was calculated using PAR<sub>30</sub> and a mean MODIS  $f_{APAR}$  calculated for each growing season for each site.

We used these time-series of tower LUE<sub>30a</sub> to calculate annual means and standard deviations of growing season midday LUE<sub>30a</sub>, where midday was defined as the period between 11:00 and 15:00 (local time). Means were calculated by averaging midday LUE<sub>30a</sub> values over the growing season, for each year.

In the case of LUE<sub>90a</sub>, PAR<sub>90</sub> was multiplied by the MODIS  $f_{APAR}$  value closest to the date of each MODIS overpass, as described in Section 2.2.2. For these 90-minute averages, no gap-filled data were used because we wanted to eliminate the possibility of introducing errors from the gap-filling procedure into the relationships between LUE and the spectral indices. For this reason, incomplete 90-minute averages (i.e., those for which there was at least one missing 30-minute value inside the 90-minute window) were rejected from the analyses. Finally, we computed annual means and standard deviations of growing season LUE<sub>90a</sub> and LUE<sub>90i</sub>. Means were calculated by averaging the LUE<sub>90a</sub> or LUE<sub>90i</sub> value at times of MODIS overpasses

**Table 3**  
Flux and meteorology datasets used in this study

| Site Code | Growing season (s) <sup>a</sup> |
|-----------|---------------------------------|
| SOBS      | 2001, 2002, 2003, 2004          |
| OJP       | 2001, 2002, 2003                |
| HJP75     | 2004                            |
| HJP94     | 2001, 2002, 2003, 2004          |
| HJP02     | 2003, 2004                      |
| F77       | 2003, 2004                      |
| F89       | 2001, 2002, 2003, 2004          |
| F98       | 2002, 2003, 2004                |

<sup>a</sup> A growing season is defined as the period between days 152 (June 1) and 243 (August 31).

**Table 4**

Parameters used in the 5-Scale model for estimating the canopy shadow fraction for each MODIS pixel

| Site  | LAI | $\Omega_E$ | $\gamma_E$ | Ha   | Hb   | D     | R    | Source |
|-------|-----|------------|------------|------|------|-------|------|--------|
| SOBS  | 3.8 | 0.90       | 1.36       | 5.44 | 5.44 | 6200  | 0.98 | 1,3    |
| OJP   | 2.6 | 0.85       | 1.42       | 8.5  | 5.5  | 1250  | 1.1  | 1,3    |
| HJP75 | 2.9 | 0.93       | 1.44       | 1.0  | 3.5  | 10700 | 0.45 | 1,2,3  |
| HJP94 | 0.8 | 0.83       | 1.44       | 0.1  | 1.4  | 5770  | 0.35 | 1,2,3  |

LAI: leaf area index ( $\text{m}^2/\text{m}^2$ );  $\Omega_E$ : needle-to-shoot ratio values;  $\gamma_E$ : clumping index (within crowns only); Ha: “stick” height (m); Hb: crown vertical size (m); D: Tree density (stems/ $\text{m}^2$ ); R: crown radius (m); Source: 1. BOREAS CD-ROM Set, 2. L. Chasmer (FCRN-DIS), 3. 5-Scale.

over the growing season, for each year. The number of observations used to calculate annual means at each site is about equal to the number of MODIS observations in each growing season.

We also derived time-series of daily-integrated sums of  $\text{LUE}_{30a}$  for comparison to means of midday  $\text{LUE}_{90a}$  values on clear days. Daily-integrated sums were calculated as the ratio of daily GEP to daily APAR, where daily GEP and daily incident PAR were calculated by multiplying each 30-minute period of gap-filled data by 1800 s and

summing, for each day, over only periods determined by the following specific conditions:

- $\text{PAR}_{30}$  greater than  $5 \mu\text{mol photons m}^{-2} \text{s}^{-1}$ ;
- $\text{GEP}_{30}$  greater than  $0 \mu\text{mol C m}^{-2} \text{s}^{-1}$  and less than a site-specific maximum value, ranging from 10 to  $35 \mu\text{mol C m}^{-2} \text{s}^{-1}$  depending on the site and determined by visual inspection of time-series of  $\text{GEP}_{30}$ .

Daily APAR was then obtained by multiplying daily incident PAR by the mean MODIS  $f_{\text{APAR}}$  for the growing season. Daily APAR and daily GEP values calculated with more than 10% of gap-filled data were excluded from subsequent analyses. For calculating means of midday  $\text{LUE}_{90a}$  on clear days, the following criteria were used:

- Periods of  $\text{PAR}_{30}$  and  $\text{GEP}_{30}$  between 11:00 and 12:30, inclusively;
- $\text{PAR}_{30}$  greater than  $1500 \mu\text{mol photons m}^{-2} \text{s}^{-1}$ ;
- Standard deviation of  $\text{PAR}_{90}$  less than  $50 \mu\text{mol photons m}^{-2} \text{s}^{-1}$ ;
- Same restrictions on  $\text{GEP}_{30}$  as for the calculation of daily sums;
- No gap-filled data.

#### 2.4. Regional map of $\text{LUE}_{90a}$

Using the relationships that we subsequently developed between PRI and LUE (see Results), we created a regional map of  $\text{LUE}_{90a}$  from a

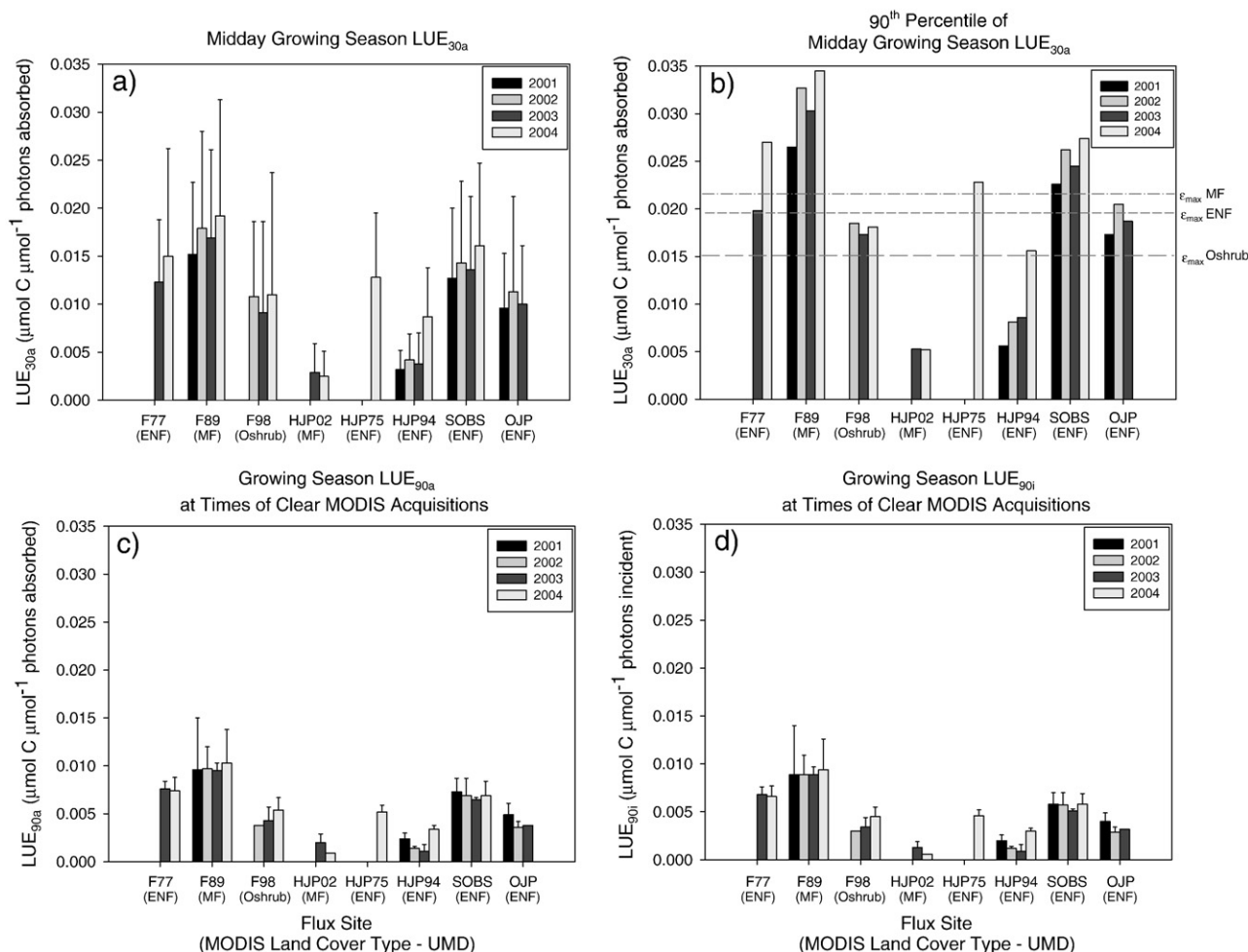


**Fig. 1.** Annual means and standard deviations of (a) midday growing season gross light-use efficiency (LUE) based on absorbed PAR calculated using 30-minute flux data ( $\text{LUE}_{30a}$ ), (b) 90th percentile of midday growing season  $\text{LUE}_{30a}$ , (c) growing season LUE at the times of clear MODIS acquisitions based on absorbed PAR calculated using an average of three 30-minute periods of flux data centered on the overpasses times ( $\text{LUE}_{90a}$ ), (d) growing season LUE at the time of clear MODIS acquisitions based on incident PAR ( $\text{LUE}_{90i}$ ). The growing season is defined as the period between day 152 and day 243 inclusively. Midday is defined here as the 30-minute periods between 11:00 and 15:00 (local time). MODIS land cover types refer to the University of Maryland classification scheme of the MOD12Q1 product used in the MODIS GPP algorithm. ENF: Evergreen Needleleaf; MF: Mixed Forests; Oshrub: Open Shrublands. Values of  $\epsilon_{\text{max}}$  in b) refer to the values used in the MODIS GPP algorithm, for the respective cover types: ENF=0.0196, MF=0.0217, Oshrub=0.0151  $\mu\text{mol C } \mu\text{mol}^{-1} \text{ photons absorbed}$ .

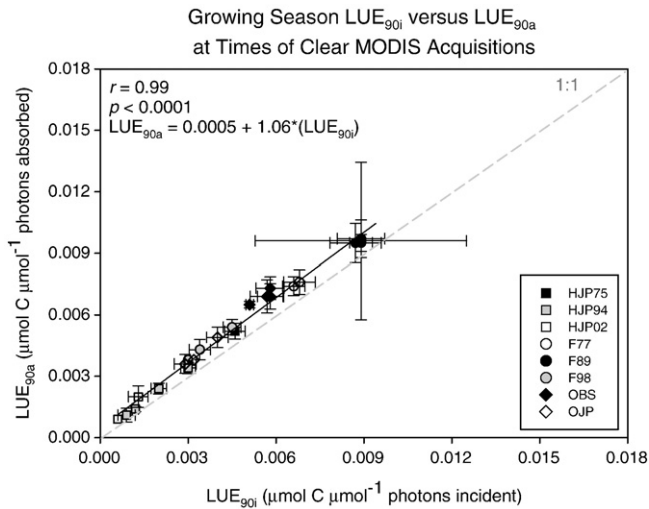


**Fig. 2.** Correlations between mean 90-minute light-use efficiency for each study site calculated using incident PAR (LUE<sub>90i</sub>) versus the mean 90-minute light-use efficiency for the same site calculated using absorbed PAR (LUE<sub>90a</sub>) for each year at the times of the clear MODIS acquisitions. Bars represent standard errors.

MODIS TOA reflectance image of the study area acquired at 12:15 (local time) on August 3, 2001. In an IDL/ENVI environment, we extracted from this image an area of about 47,500 km<sup>2</sup> encompassing all flux towers. We used the MODIS land cover map to create a mask that excluded all pixels that were not classified as one of the three biome-level cover types assigned to the flux towers. Using the same classification scheme, along with vector hydrology data, we also included in this mask all pixels corresponding to water bodies or rivers. The mask was then applied to the TOA reflectance image, and also to a co-registered MODIS AOT image for the same date. TOA for each pixel in the masked image was atmospherically corrected to surface reflectance using 6S and the corresponding AOT. Prior to atmospheric correction, all missing values in the AOT image were gap-filled using the GS+ geostatistical package (version 7) and an ordinary kriging interpolation method. Finally, the PRIs were derived for each pixel of the surface reflectance image and LUE<sub>90a</sub> was calculated using one of the models derived in this study.

For the same date and region, we created a map of daily LUE<sub>a</sub> for the three cover types (ENF, MF, and Oshrub) using the same method as the one used operationally by the MODIS GPP algorithm to calculate daily LUE (Heinsch et al., 2003). We compared this map to our MODIS PRI-derived map of LUE<sub>90a</sub>.

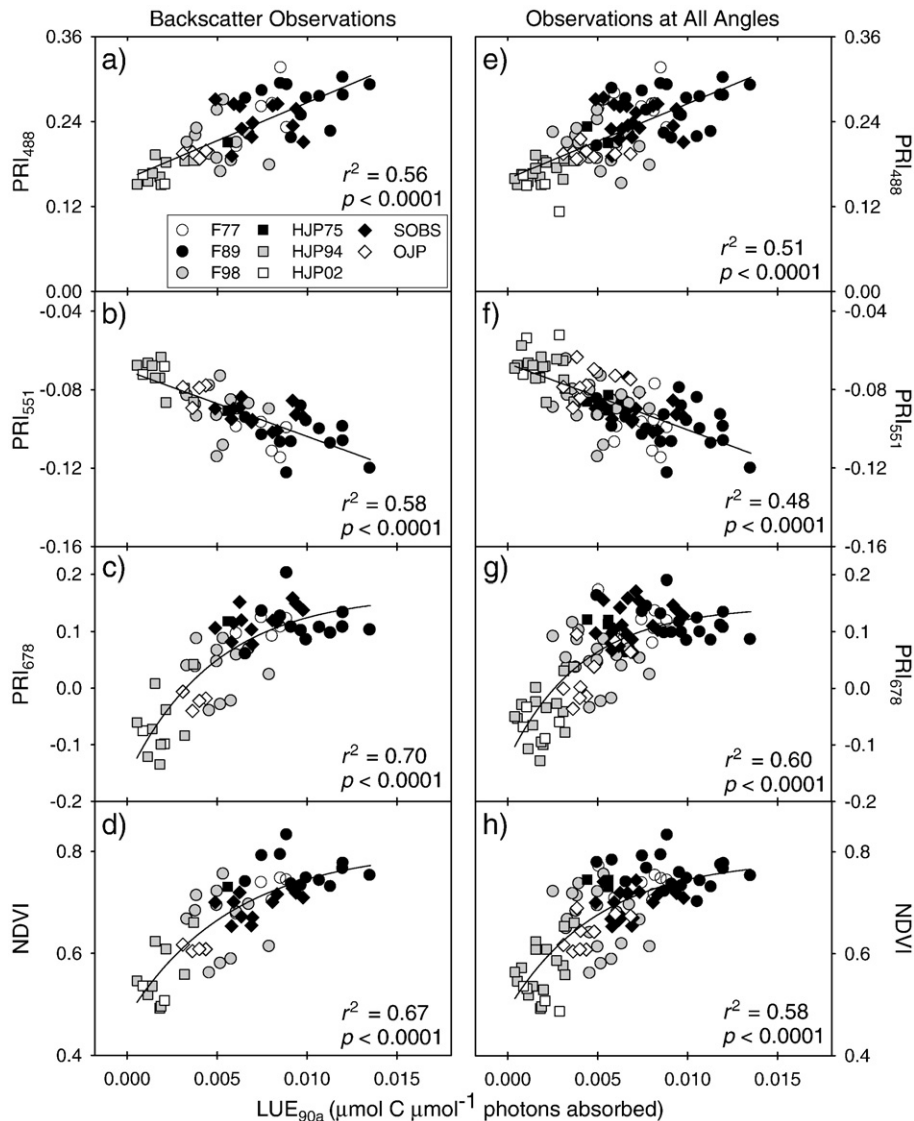


**Fig. 3.** Relationships of the PRIs using reference bands at 488 nm, 551 nm, and 678 nm and NDVI, with 90-minute LUE from flux towers, for (a–d) observations close to the backscattering direction, and (e–h) observations at all view angles (see Table 5 for equations of fitted lines).

**Table 5**

Regression parameters for the relationships between tower-derived 90-minute gross  $LUE_{90a}$ , and different formulations of the MODIS PRI and the NDVI

| Model  | All observations ( $n=99$ ) |       |        |       | Backscatter only ( $n=57$ ) |       |        |       |
|--|-----------------------------|-------|--------|-------|-----------------------------|-------|--------|-------|
|  | $a$                         | $b$   | $c$    | $r^2$ | $a$                         | $b$   | $c$    | $r^2$ |
| $PRI_{488} = aLUE_{90a} + b$                       | 10.60                       | 0.16  | –      | 0.51  | 10.75                       | 0.16  | –      | 0.56  |
| $PRI_{551} = aLUE_{90a} + b$                       | –3.39                       | –0.07 | –      | 0.48  | –3.35                       | –0.07 | –      | 0.58  |
| $PRI_{678} = a + b$<br>( $1 - \exp(-cLUE_{90a})$ ) | –0.13                       | 0.27  | 242.39 | 0.60  | –0.16                       | 0.32  | 204.46 | 0.70  |
| $NDVI = a + b$<br>( $1 - \exp(-cLUE_{90a})$ )      | 0.49                        | 0.30  | 198.75 | 0.58  | 0.47                        | 0.33  | 171.81 | 0.67  |

All regressions are significant at the  $\alpha=0.01$  level.

## 2.5. Geometric-optical modeling

To examine the effect of view and illumination angles on PRI values, canopy shadow fraction was derived for each extracted tower pixel using the 5-Scale geometric-optical model (Leblanc & Chen, 2000). The pixel shadow fraction corresponds to the fractional area inside a pixel where tree crowns are shaded by adjacent trees and thus receive only diffuse light. The 5-Scale model was parameterized with MODIS view and illumination angles associated with each pixel, and biometric measurements made at the flux sites (Table 4). Only four out of our eight study sites were used for this analysis because of the limitations of the model in producing consistent shadow fraction estimates at sites with more complex canopies such as those of the burned sites, or stands at early stages of succession such as the HJP02 site.

## 2.6. Statistical analyses

Matlab (version 7.1) was used for calculating descriptive statistics of growing season midday  $LUE_{30a}$ , and  $LUE_{90i}$  and  $LUE_{90a}$  at times of MODIS overpasses. ANOVAs were carried out using SAS's (version 9.1.3) GLM procedure (SAS Institute Inc., 2000). Linear and non-linear regression analyses were performed using the SigmaPlot statistical and plotting package version 8.02 (SPSS, 2002) to study the relationships between the MODIS spectral indices, tower  $LUE_{90a}$  and  $LUE_{90i}$ , and canopy shadow fraction.

## 3. Results

### 3.1. Inter-site and inter-annual differences in tower LUE

Within each site, there were significant differences in the annual means of midday growing season for  $LUE_{30a}$  (all  $p$ -values  $\leq 0.016$ ) and the variability was relatively large in each year (Fig. 1a), with coefficients of variation (COV) ranging between 49% and 115%. There were also significant differences among the sites except between F77 and SOBS, and between F98 and OJP. The F89 site had the highest mean  $LUE_{30a}$  and exhibited the largest variability. At the other extreme, the recently cutover HJP02 site had the smallest mean  $LUE_{30a}$  and showed little variability within a growing season. There were also some major differences in  $LUE_{30a}$  for sites within the same land cover class. For example, the F89 and HJP02 sites, both in the MF land cover class, displayed large differences in their respective  $LUE_{30a}$ . There were also large differences in  $LUE_{30a}$  within the ENF cover type for which the HJP94 site was lower than the SOBS and F77 sites.

### 3.2. Tower LUE and MODIS BPLUT $\epsilon_{max}$

We compared 90th percentiles of midday tower  $LUE_{30a}$  to the biome-specific maximum LUE values ( $\epsilon_{max}$ ) used in the MOD17 GPP algorithm as described in the BPLUT of the MOD17 User's Guide (Heinsch et al., 2003). At a few sites (F77, F89, F98, HJP75, and SOBS),

$LUE_{30a}$  reached higher values during the growing season than the corresponding  $\epsilon_{max}$  values for their respective cover types (Fig. 1b). For other sites, such as the HJP02 and HJP94 sites,  $LUE_{30a}$  always remained well below the BPLUT  $\epsilon_{max}$  value (Fig. 1b).

### 3.3. Comparing tower $LUE_{30a}$ with tower $LUE_{90a}$ and $LUE_{90i}$

We next compared the 90-minute LUE values at the times of the clear MODIS acquisitions ( $LUE_{90a}$  and  $LUE_{90i}$ ) to the 30-minute midday average LUE obtained over the entire growing season ( $LUE_{30a}$ ) (Fig. 1c–d versus a). Compared to  $LUE_{30a}$  (Fig. 1a), the magnitudes of mean growing season  $LUE_{90a}$  and  $LUE_{90i}$  at the times of the clear MODIS acquisitions were lower at all sites (Fig. 1c–d). Again, the F89 site showed greater mean  $LUE_{90a}$  and  $LUE_{90i}$  as well as greater variability than the other sites. Variability of  $LUE_{90a}$  and  $LUE_{90i}$  was also lower at all sites compared to that for  $LUE_{30a}$  (COVs between 4%–70% versus 49%–115%). The pattern for relative differences in  $LUE_{90a}$  and  $LUE_{90i}$  (Fig. 1c–d) among sites was similar to those observed for  $LUE_{30a}$  (Fig. 1a).

### 3.4. Comparison of tower $LUE_{90i}$ to $LUE_{90a}$

As mentioned in Section 2.3.1, reliable and continuous estimates of  $f_{APAR}$  are difficult to obtain (Zhao et al., 2005). To determine the extent to which including  $f_{APAR}$  might cause problems, we compared calculations

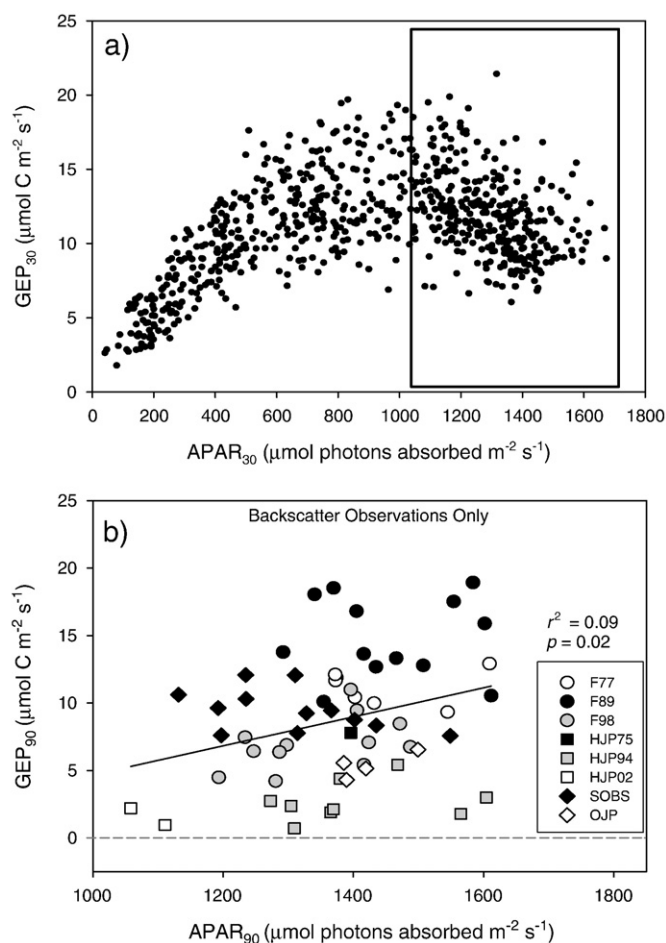


**Fig. 4.** (a) Typical light-response curve from 30-minute flux tower measurements made at the F89 fire site for a single growing season. The rectangle delimits the approximate ranges of  $GEP_{30}$  and  $APAR_{30}$  at the times when flux measurements are concomitant with MODIS acquisitions. A single mean  $f_{APAR}$  value for this site and growing season were used. (b) Relationship between  $GEP_{90}$  and  $APAR_{90}$  for all sites at times when the clear MODIS acquisitions were close to the backscatter direction.



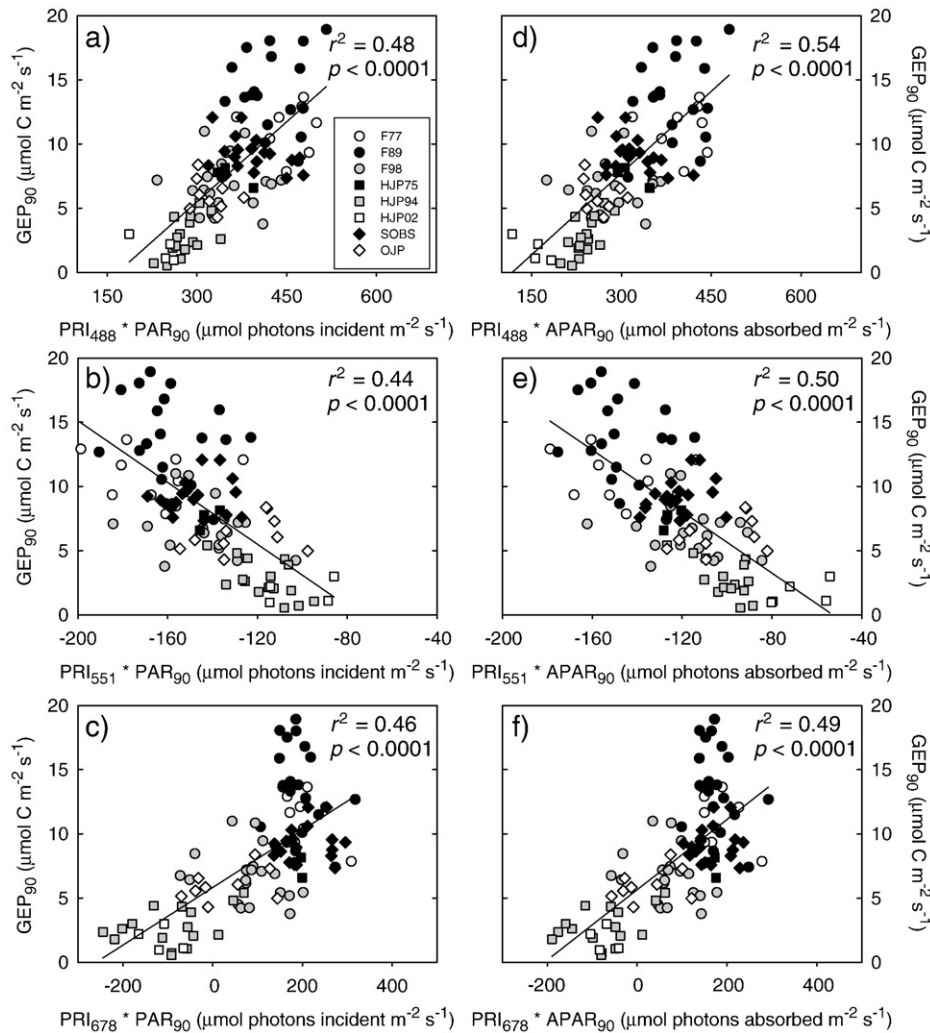


**Fig. 5.** Relationship between (a–c)  $GEp_{90}$  and  $PRI \cdot PAR_{90}$ , and (d–f)  $GEp_{90}$  and  $PRI \cdot APAR_{90}$ , for different formulations of PRI, at times of clear MODIS acquisitions using data from all sensor and illumination directions.

of LUE based on both incident and absorbed PAR (i.e.,  $LUE_{90i}$  versus  $LUE_{90a}$ ). Mean  $LUE_{90i}$  values at the times of the MODIS acquisitions were systematically lower than those for  $LUE_{90a}$  (Fig. 1c–d) for any given site and the two measures of LUE were strongly correlated ( $r=0.99$ ) at the times of clear MODIS acquisitions (Fig. 2). The MODIS  $f_{APAR}$  values we used averaged 0.82 for all sites and were generally fairly stable over the course of the growing season at the coniferous sites.  $LUE_{90a}$  was slightly greater than  $LUE_{90i}$  and the strong correlation allowed us to compute the seasonal average across all sites as:  $LUE_{90a} = c + m \cdot (LUE_{90i})$ . This provided a means to estimate  $LUE_{90a}$  when only  $LUE_{90i}$  was available, and was needed for determinations of daily LUE (see below). However, analyses of the impact of using Eqs. (1) or (2) to calculate LUE (Figs. 1c–d, 2) determined that the difference between the two calculation methods was negligible as was its influence on the subsequent analyses. Consequently, we henceforth use only LUE based on APAR because it has a stronger biological basis.

### 3.5. MODIS PRI and NDVI versus LUE

We analyzed our dataset of MODIS PRIs and NDVI using (1) only observations close to the backscattering direction (i.e., the difference between sun and sensor azimuth angles was less or equal to  $60^\circ$ ), and (2) all observations. We found no significant correlations between any of the MODIS spectral indices and  $LUE_{90a}$  when we examined individual sites. However, we found moderate to strong correlations when data

from all sites were combined (Fig. 3). The correlation between PRI using reference band 13 at 667 nm ( $PRI_{667}$ ) and  $LUE_{90a}$  was similar to that obtained for a PRI using reference band 14 at 678 nm ( $PRI_{678}$ ). For this reason, we excluded  $PRI_{667}$  from subsequent analyses.

In all cases, the correlation between a spectral index and  $LUE_{90a}$  was improved when only observations closer to the backscatter direction were used (Fig. 3a–d) compared to when observations acquired at all sensor and illumination angles were used (Fig. 3e–h). Relationships between  $LUE_{90a}$  and spectral indices calculated from top-of-the-atmosphere (TOA) reflectances were weaker than for those calculated using surface reflectances ( $r^2$  values around 0.02 for TOA versus 0.5–0.6 for surface reflectances, depending on the reference

**Table 6**

Regional and fractional areas covered by the cover types representative of the flux sites used in this study

| Cover type                        | Area (km <sup>2</sup> ) | Fraction of study area (%) |
|-----------------------------------|-------------------------|----------------------------|
| Evergreen needleleaf forest (ENF) | 31 586                  | 66.6                       |
| Mixed forest (MF)                 | 6 597                   | 13.9                       |
| Open shrubland (Oshrub)           | 806                     | 1.7                        |
| Masked <sup>a</sup>               | 8 439                   | 17.8                       |
| Total                             | 47 428                  | 100.0                      |

<sup>a</sup> Masked pixels include pixels classified as water or cover types not represented by the flux sites.

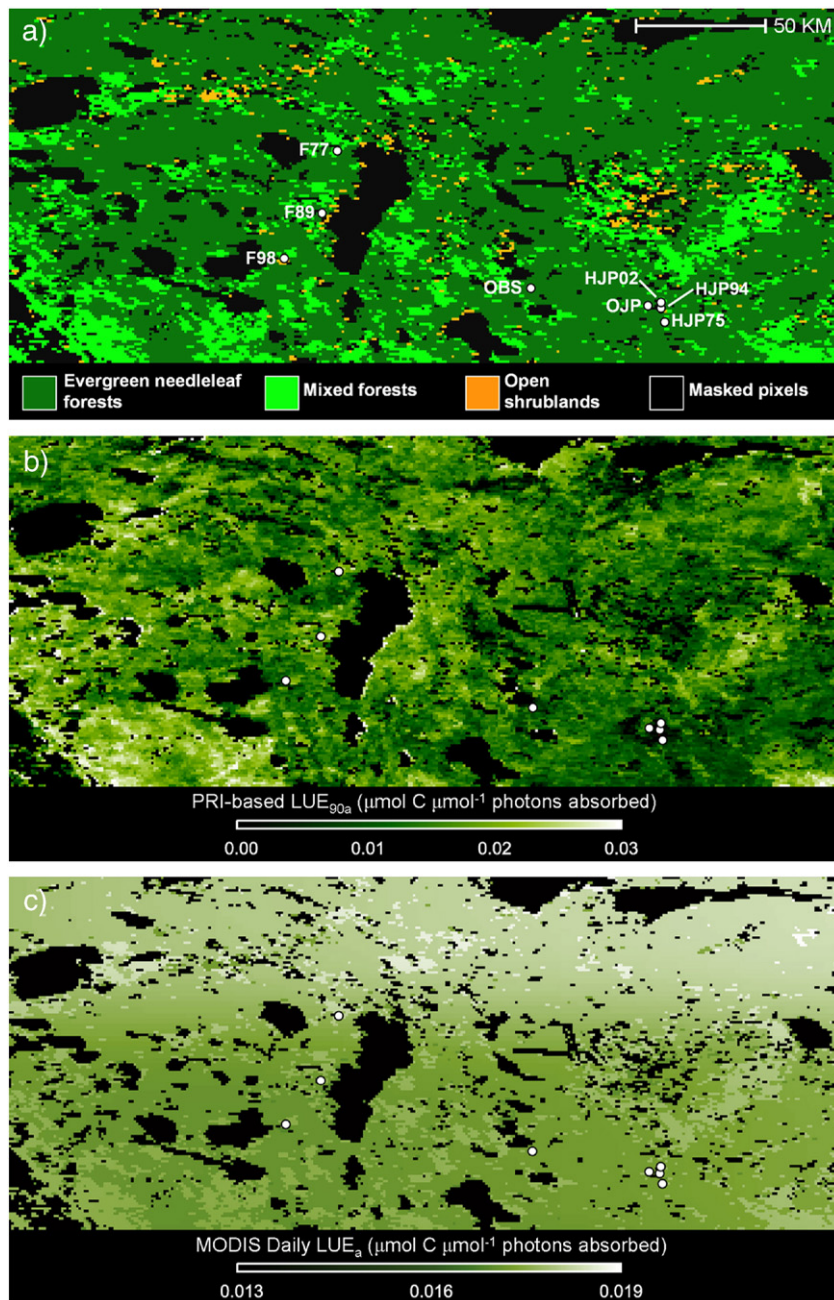


**Fig. 6.** (a) MOD12Q1 land cover classification (UMD) of the BERMS region showing only those pixels classified as evergreen needleleaf forests, mixed forests, and open shrublands. All other cover types and water surfaces were masked out. The locations of the flux towers used in this study are shown as white circles. (b) LUE map of the study area derived from the relationship between  $PRI_{551}$  and  $LUE_{90a}$  (Note that lighter areas have higher LUE). (c) LUE map of the study area derived using the MOD17 approach (i.e.,  $LUE = f(\epsilon_{max}, VPD, T_{min})$ ), for the same day.

bands used). We found a positive linear relationship between  $PRI_{488}$  and  $LUE_{90a}$  (Fig. 3a and e, Table 5). Conversely, we found a negative linear relationship between the  $PRI_{551}$  and  $LUE_{90a}$  (Fig. 3b and f, Table 5). However, the strengths of these linear relationships did not differ significantly between the two models. Interestingly, NDVI and  $PRI_{678}$  both showed similar relationships with  $LUE_{90a}$  (Fig. 3c–d, and g–h). Unlike  $PRI_{488}$  and  $PRI_{551}$ , NDVI and  $PRI_{678}$  both showed positive curvilinear relationships with  $LUE_{90a}$ .

### 3.6. Predicting GEP from APAR and PRI

We examined the effect of adding a MODIS-derived PRI to  $PAR_{90}$  (or  $APAR_{90}$ ) on the prediction of  $GEP_{90}$ . Our flux measurements coincident with clear MODIS observations had a range of APAR

between about 1000 and 1700  $\mu\text{mol m}^{-2} \text{s}^{-1}$ . Fig. 4a shows a typical light-response curve for 30-minute estimates of GEP and APAR derived from flux tower measurements and MODIS  $f_{APAR}$  for one of the study sites (F89). The window inside Fig. 4a indicates the APAR region for which we had clear MODIS images concomitant with tower data. In this APAR region on clear days,  $LUE_{30a}$  had very low values. None of the sites had a significant relationship between  $GEP_{90}$  and  $APAR_{90}$  for tower data coincident with clear MODIS observations (Fig. 4b).

When  $PAR_{90}$  was multiplied by any of the three formulations of MODIS PRI, however, it explained almost 50% of the variation in  $GEP_{90}$  (Fig. 5a–c). Moreover, when any of the MODIS PRI's were multiplied by  $APAR_{90}$  instead of  $PAR_{90}$ , the model's capacity to predict  $GEP_{90}$  was further increased (Fig. 5d–f).

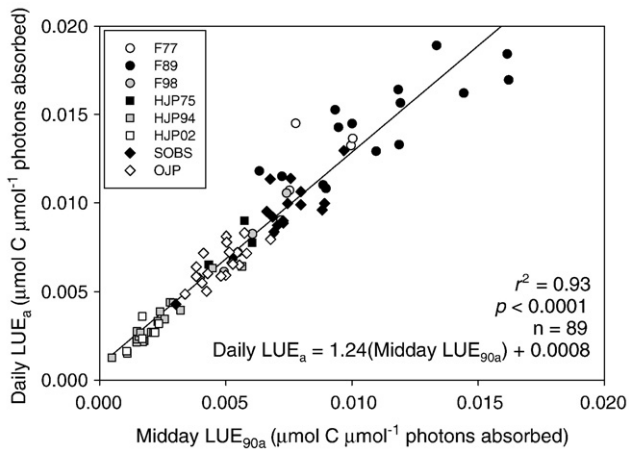


**Fig. 7.** Relationship between midday  $LUE_{90a}$  (between 11:00 and 12:30, local time) and daily  $LUE_a$ . Daily  $LUE_a = 1.24(\text{Midday } LUE_{90a}) + 0.0008$ .

### 3.7. Regional LUE map

The ENF, MF, and Oshrub cover types covered 66.6%, 13.9%, and 1.7%, respectively, of the study area (Table 6 and Fig. 6a). The remaining 17.8% of the area was covered by water bodies and other cover types that were not associated with any of the flux sites used in this study. We used one of the models we developed between MODIS PRI observations closer to the backscatter direction and  $LUE_{90a}$  (Table 5),

$$LUE_{90a} = \frac{PRI_{551} + 0.07}{-3.35},$$

to create a map of 90-minute gross light-use efficiency for the study area (Fig. 6b). We chose the  $PRI_{551}$  model for two major reasons. First, although the  $PRI_{678}$  was more strongly correlated to  $LUE_{90a}$  ( $r^2 = 0.7$ ), it was similar to the  $NDVI-LUE_{90a}$  relationship and it saturated at high LUE values (Fig. 3). Second, the  $PRI_{551}$  model had less scatter in its relationship with  $LUE_{90a}$  than did  $PRI_{488}$  (Fig. 3). Moreover, the  $PRI_{551}$  uses a reference band that is closer to the reference band that has been used in other PRI studies (570 nm). In the  $PRI_{551}$ -derived  $LUE_{90a}$  map, 161 pixels (0.3% of the study area) had negative LUE values. These values corresponded mostly to water pixels that were not captured by the mask and also to riparian and very humid zones (wetlands,

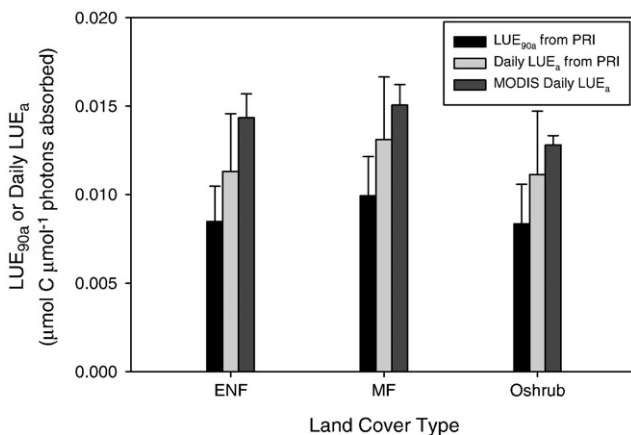


**Fig. 8.** Means and standard deviations of  $LUE_{90a}$  from PRI and daily  $LUE_a$  from PRI for the ENF, MF, and Oshrub cover types as derived from the LUE map for day 215 of year 2001 (Fig. 6b). Also, daily  $LUE_a$  obtained from the MODIS GPP algorithm (Fig. 6c). Daily  $LUE_a$  from PRI was derived from the relationship between midday  $LUE_{90a}$  (between 11:00 and 12:30) and daily  $LUE_a$  (see Fig. 7).

submerged lands, etc.). We did not include these 161 pixels in calculations of the statistics for each cover type (Fig. 8).

We compared our regional  $LUE_{90a}$  map to a daily LUE map derived for the same date using the standard MODIS GPP approach (Fig. 6c) where maximum LUE was scaled down as a function of VPD and air temperature constraints. Not surprisingly, this map showed less spatial variability than our MODIS PRI-derived  $LUE_{90a}$  map. We used the relationship derived between midday  $LUE_{90a}$  on clear days and daily  $LUE_a$  (Fig. 7) to transform the MODIS PRI-derived  $LUE_{90a}$  from the map (Fig. 6b) into daily  $LUE_a$ . This permitted further comparison of the means and standard deviations with those from the MODIS GPP daily LUE map (Fig. 8). Again, we found that the variability in PRI-derived  $LUE_{90a}$  and PRI-derived daily  $LUE_a$  was greater than that of the MODIS GPP-derived  $LUE_a$  (Fig. 8) over the study area. Furthermore, daily LUE derived using the  $PRI_{551}$  index provided estimates similar to those computed using the standard MODIS LUE product (Fig. 8). However, both methods for deriving daily LUE values were consistent in terms of the relative differences in LUE among the three cover types.

### 3.8. Relationship between pixel shadow fraction, MODIS PRI, and tower LUE

For a subset of four sites (SOBS, OJP, HJP75, and HJP94) for which we had enough auxiliary information to run the 5-Scale model, the relationships between canopy shadow fraction and the three formulations of the MODIS PRI (Fig. 9) were found to be similar to the relationships found previously between PRI and  $LUE_{90a}$  (Fig. 3).

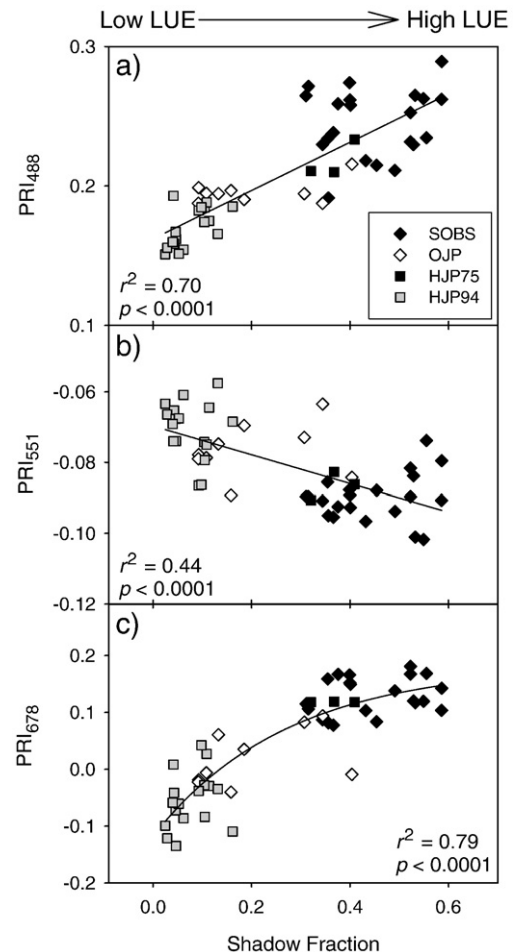


**Fig. 9.** Relationships between MODIS PRI and canopy shadow fraction derived from the 5-Scale model for three different formulations of the PRI.



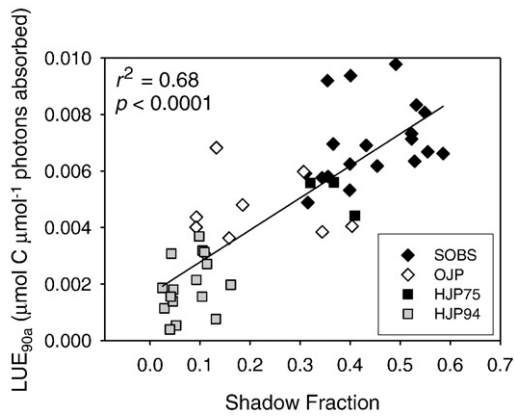


**Fig. 10.** Relationships between tower  $LUE_{90a}$  and canopy shadow fraction derived from the 5-Scale model.

The PRIs using reference bands at 488 nm and 551 nm showed positive and negative linear relationships with canopy shadow fraction, respectively (Fig. 9a–b). The PRI using the reference band at 678 nm showed a positive curvilinear relationship with shadow fraction. In all cases, the study sites with lower canopy shadow fractions also corresponded to the sites with the lower LUE values, and vice-versa. This is shown in Fig. 10 where the SOBS site had high  $LUE_{90a}$  values corresponding to high canopy shadow fractions whereas the HJP94 site had lower  $LUE_{90a}$  values and lower shadow fractions.

## 4. Discussion

### 4.1. Magnitude and variability of tower $LUE_{30a}$

The magnitude and variability of continuous midday  $LUE_{30a}$  measured at the tower sites (Fig. 1a) are comparable to other values found in the literature. However, direct comparisons are complicated by the use of different definitions of LUE in different studies (e.g., net/gross, growing season/annual, incident/absorbed PAR, photons/joules, etc. [Gower et al., 1999]). Coursolle et al. (2006), for example, reported similar values of gross LUE based on incident PAR for several of the same study sites for August 2003. Similar values of LUE, which ranged between 0.01 and 0.04  $\mu\text{mol C } \mu\text{mol}^{-1}$  photons absorbed, have been reported for other boreal and temperate forests (Jenkins et al., 2007; Schwalm et al., 2006; Turner et al., 2003, 2005).

At short (diurnal, daily) to moderate (monthly, seasonal) time scales, variations in LUE can be attributed in large part to variations in the ratio of diffuse to direct PAR irradiance (Gu et al., 2002; Jenkins et al., 2007) caused by the passage of clouds, by changes in atmospheric aerosols, and by the diurnal course of solar elevation (Ni et al., 1997). An increase in this ratio raises the level of light penetration into the canopy and enhances LUE (Coursolle et al., 2006; Gu et al., 2002; Hollinger et al., 1994). Conversely, longer-term variability in growing season LUE (e.g., inter-annual, decadal) is driven more by extreme environmental conditions, such as extended periods of drought or heat waves, thus reducing LUE through recurrent high vapor pressure deficits (VPD), high temperatures, and low soil moisture content (Barr et al., 2007; Ciais et al., 2005; Nouvellon et al., 2000). Inter-annual variations in  $f_{APAR}$  resulting from such unfavorable conditions (Ciais et al., 2005) also affect the variability of LUE.

The large differences observed in  $LUE_{30a}$  among our study sites are consistent with differences reported by Ahl et al. (2004) for net LUE (Net Ecosystem Production/APAR) of different cover types of northern hardwood forests. Similar between-site differences in gross LUE were also reported by Schwalm et al. (2006) for many of our study sites for

2004. These differences can be explained mostly by the variations in species composition (Whitehead & Gower, 2001), age, and tree architecture among the study sites. Note that some of the larger differences between  $LUE_{30a}$  are at sites having the same cover type classification (e.g., F89 versus HJP02). A possible explanation for these differences could be in misclassification of pixel-level cover types. For example, the HJP02 site was classified as a mixed forest (MF) although it was planted exclusively with jack pine and likely would be better classed as Oshrub. Such misclassification errors can introduce large uncertainties into the outputs from GPP algorithms based on remote sensing inputs (Zhao et al., 2005) and this highlights the importance of assigning accurate cover type information to input pixels. A direct remote sensing-based measurement of LUE, such as the one explored in this paper, could help resolve this reliance on accurate cover type information.

### 4.2. Comparison of tower LUE with MODIS BPLUT $\epsilon_{max}$ values

Tower-based  $LUE_{30a}$  values at some of our study sites exceeded their corresponding  $\epsilon_{max}$  values from the MOD17 BPLUT (e.g., F89, SOBS) (Fig. 1b) and this suggested another source of inaccuracy in the MODIS GPP algorithm when it was applied to northern ecosystems (Turner et al., 2005). The differences observed between tower  $LUE_{30a}$  values and their MOD17  $\epsilon_{max}$  values at some of the study sites indicated that LUE-based GPP algorithms need to more accurately represent the spatial heterogeneity and temporal range of LUE across the landscape (Trotter et al., 2001). Once again, a direct spectral measurement of LUE could help resolve this problem.

Conversely, the small  $LUE_{30a}$  values observed at the HJP94 and HJP02 sites, compared to their respective BPLUT  $\epsilon_{max}$  values (Fig. 1b), could be explained by over-estimated MODIS  $f_{APAR}$  values used to calculate  $LUE_{30a}$ . One reason is that large differences exist in spatial resolution between ground measurements (e.g., 1–10 m) and MODIS  $f_{APAR}$  estimates (~500 m). For example, MODIS  $f_{APAR}$  for the HJP94 site (0.71–0.89) were much greater than the green  $f_{APAR}$  measured by Chen et al. (2006) at this site (0.22). However, green  $f_{APAR}$  represents the fraction of PAR absorbed by the foliage only, while the reflectance-based MODIS  $f_{APAR}$  includes ground vegetation as well as possible contributions from non-photosynthetic (e.g., standing and leaf litter, woody stems, etc.) vegetation. Uncertainties related to the MODIS  $f_{APAR}$  contribute to the overall uncertainty in remote sensing-based GPP estimates. However, these uncertainties need to be included in our current analysis if we are to obtain an accurate initial assessment of the consequences of introducing a MODIS-based PRI into the MODIS GPP algorithm. The initial test reported here for a chronosequence of boreal forest sites appeared to work quite well.

### 4.3. $LUE_{30a}$ versus $LUE_{90a}$ and $LUE_{90i}$ at the times of MODIS overpasses

The dramatic reduction in magnitude and variability of  $LUE_{90a}$  for the times of clear midday MODIS overpasses (Fig. 1c–d) compared to the variability in continuous  $LUE_{30a}$  (Fig. 1a) was similar to results reported by Drolet et al. (2005) and Sims et al. (2005). This reduction, attributed to light-saturating conditions for photosynthesis that prevail at midday on clear days, significantly decreases the potential of space-based optical remote sensing data to directly track changes in LUE at short and moderate time scales. Separating the overpass times of future dual-sensor missions (e.g., MODIS on Terra and Aqua) by longer time intervals over the course of a day could help circumvent this problem. Furthermore, a geostationary sensor capable of near-continuous reflectance measurements would also be a way of making more general estimates of LUE using remote sensing. Although most of the variability in  $LUE_{30a}$  disappeared at times of clear MODIS overpasses, between-site differences in  $LUE_{90a}$  were still present (Fig. 1a versus c). This suggests that the direct detection of temporal variations in the LUE at these sites is unlikely using only clear MODIS images. Furthermore, it indicates that the use of MODIS spectral



indices to capture regional-scale variations in LUE may be limited to detecting minimum LUE values related to cover type or successional stage. Nevertheless, we believe that there are efficient means to gap-fill from these minimum LUE values to other periods using climate and radiation data and this will be the focus of future studies.

#### 4.4. Relationships between MODIS spectral indices and tower LUE

While several studies have shown that PRI was successful in tracking variations in LUE at the leaf, plant, and small canopy scale (e.g., Filella et al., 1996; Gamon et al., 1992; Nichol et al., 2000; Rahman et al., 2001), its use at the scale of MODIS ocean band pixels ( $\geq 1 \text{ km}^2$ ) represents a significant challenge. Several factors associated with the design of the satellite mission and with sensor characteristics, as well as factors associated with the measurement and processing of eddy covariance data, contribute to this complexity. A major issue is the reduced range in canopy LUE at times of the MODIS overpasses (Fig. 2c–d) which generally occur between noon and 14:00 (local time) at the study area (Drolet et al., 2005). Additionally, Barton & North (2001) used a ray-tracing model to show that soil background, canopy structural attributes (e.g., LAI, leaf angle distribution), view/illumination angles, and the accuracy of the atmospheric correction are all factors that can obscure the subtle variations of PRI with LUE. For example, variations in view and illumination angles may cause the sensor to measure reflectances from leaves illuminated at different light intensities at different times thus yielding different PRIs for a given overall canopy LUE value (Barton & North, 2001). This could explain the strong relationships we found between  $\text{LUE}_{90a}$  and MODIS indices when we used only observations closer to the backscattering direction (Fig. 3a–d), where all leaves were relatively well-illuminated compared to when observations at all angles were used (Fig. 3e–h). Conversely, there could be a decoupling between the physiological status of the over- and understory species, which could result in a lack of correlation between canopy reflectance and physiological status (Hill et al., 2006). Most of our flux sites had well developed photosynthetically active ground cover.

The variability in pixel size and location caused by the varying view zenith angles between MODIS images is another confounding factor that can result in measuring the reflectance of different landscape components from one MODIS acquisition to another. This problem is greatest in non-homogeneous, patchy landscapes (e.g., the areas associated with the jack pine chronosequence) and can be further amplified by pixel geolocation errors ( $\sim 50 \text{ m}$ ). Another source of uncertainty that could affect the relationships between MODIS PRIs and tower LUE arises from the measurement errors related to the MODIS instrument. According to pre-launch calibration data, the absolute radiometric accuracies for MODIS radiance and reflectance are  $\pm 0.5\%$  and  $\pm 0.2\%$ , respectively (Barbieri et al., 1997). A recent on-orbit calibration analysis of the Terra-MODIS instrument reported an annual decrease in sensor response of less than 1% since the launch date for the reflective solar bands located at wavelengths greater than 500 nm (Xiong et al., 2007). Lastly, data acquired using the eddy covariance method is also subject to uncertainties related, in part, to the method itself (e.g., sampling frequency, instrument failures, advection) but also to the post-processing of the flux data (i.e., gap-filling of missing data and flux partitioning of NEP into GEP and ecosystem respiration) (e.g., Goulden et al., 1996). However, it appears that uncertainties in the eddy covariance measurements are likely to be small compared to the satellite-related uncertainties mentioned above.

While the different MODIS PRIs extracted from the MODIS images used in this study did not allow us to detect diurnal LUE variations related to the xanthophyll cycle, they did allow us to detect spatial variations in LUE at the regional scale due to successional stage and species composition. Based on MODIS and tower data alone, it is not possible to determine to what extent variations in PRI might be related to factors such as differences in biomass, structure, canopy chlorophyll

and nitrogen content, or carotenoid/chlorophyll pigment ratios that are also correlated with LUE. Clearly, further measurements (pigment concentration, reflectance, photosynthesis, etc.) at a higher spatial resolution are needed to elucidate such relationships. The PRI:LUE relationships we found across the flux sites agree with results from other studies at the plant level that also reported strong LUE:PRI relationships across species and nutrient status (Gamon et al., 1997; Nichol et al., 2000; Rahman et al., 2001; Trotter et al., 2002). However, this is the first time to our knowledge that this relationship has been demonstrated across the landscape using a spaceborne sensor.

When comparing Fig. 4b to Fig. 5a–f, it is clear that multiplying a MODIS-derived PRI by incident  $\text{PAR}_{90}$  or  $\text{APAR}_{90}$  significantly improved the predictive power of the models to estimate  $\text{GEP}_{90}$  at high irradiance levels. Serrano & Penuelas (2005) also reported similar improvements to predictions of LUE and net  $\text{CO}_2$  uptake when PAR was multiplied by a transmittance-based PRI, indicating the influence of both structure ( $f_{\text{APAR}}$ ) and function (PAR) on carbon assimilation. Additionally, the slight improvements we observed when using  $\text{APAR}_{90}$  instead of  $\text{PAR}_{90}$  for predicting  $\text{GEP}_{90}$  (Fig. 5d–f) further demonstrate the importance of canopy structure as modulated through the  $f_{\text{APAR}}$  term in determining ecosystem productivity. It is worth noting, however, that boreal ecosystems often have a significant portion of their photosynthetic capacity located in their groundcovers such as sphagnum or moss (Kolari et al., 2006; Heijmans et al., 2004; Morén & Lindroth, 2000). Determining how a two-tiered photosynthetic structure influences the interpretation of spectral indices such as PRI is an interesting topic for future study.

#### 4.5. MODIS PRI-derived gross LUE map

Our map of  $\text{LUE}_{90a}$  derived from the MODIS  $\text{PRI}_{551}$  has shown greater spatial heterogeneity in LUE than the LUE derived using the MOD17 approach (Figs. 6b, 8). The spatial pattern of  $\text{LUE}_{90a}$  in Fig. 6b appears to be more natural than the apparent gradient present in the MOD17 approach (Fig. 6c), where the pattern of daily  $\text{LUE}_a$  values across the region is directly linked to the land cover classes (Fig. 6a) and to the GMAO climate dataset. Furthermore, our map eliminates the uncertainties associated with land cover classification (misclassifications and mixed pixels), with the BPLUT  $\varepsilon_{\text{max}}$  limitations on LUE, and with GMAO meteorological inputs (Zhao et al., 2005). The trends in the magnitudes of MODIS-derived  $\text{LUE}_{90a}$  and daily  $\text{LUE}_a$  for the three cover types (Fig. 8) are consistent with previous results for GPP for the same cover types (see Zhao et al., 2005, Fig. 7).

There will still be limitations to the operational use of such an LUE map for modeling GPP that we expect to resolve in the near future. First, a further validation of our MODIS-derived  $\text{LUE}_{90a}$  estimates would be desirable. Second, the BOREAS-SSA Old Aspen (OA) site was excluded from our models although deciduous forests occupy a large fraction of the boreal landscape and would need to be included in continental-wide GPP simulations. Thus, we need additional work exploring the PRI:LUE relationship for deciduous stands. Third, the small number of pixels (0.3%) with negative  $\text{LUE}_{90a}$  values requires additional investigation to determine their cover type. Finally, and perhaps most importantly, MODIS PRI-derived LUE values represent only snapshots of minimum midday LUE values. As mentioned above, gap-filling strategies for the time periods without clear MODIS imagery need to be developed. Such methods could use, for example, a relationship between LUE and diffuse radiation to upscale LUEs from MODIS PRI using remote sensing-derived proxies for diffuse irradiance. This will be a focus of our future work.

#### 4.6. Shadow fraction vs. PRI and LUE

The relationships between the PRIs and canopy shadow fraction (Fig. 9) are similar to those found in Fig. 3 between MODIS spectral indices and tower  $\text{LUE}_{90a}$ . They tend to confirm our hypothesis that

the sites with lower shadow fraction (SF) are associated with lower LUE and vice-versa (Fig. 10). This can be explained by the lower photosynthetic rates that usually occur in more open, less-shadowed canopies (Sims et al., 2005) such as HJP94. Since the absorbed radiation in these canopies is largely composed of direct beam irradiance, with negligible diffusion inside the canopy, most of the photosynthesis occurs under light-saturated conditions. On the other hand, denser stands are subject to greater light penetration through the canopy, resulting in more photosynthesis that occurs under non-saturating conditions. Another factor to consider is the relationship between PRI and LAI. Generally, forest stands having a low LAI and thus a low SF tend to have more exposed soil background which has a direct effect on PRI (Barton & North, 2001).

Using spectral mixture analyses along with allometry, Hall et al. (1995) and Peddle et al. (1999) found positive correlations between SF, biomass density, and biophysical attributes related to photosynthetic activity (e.g., LAI, NPP, etc.) of black spruce stands. Hall et al. (1995) also found a weak curvilinear relationship between NDVI and SF ( $r^2=0.23$ ) similar to the relationship we found between PRI<sub>678</sub> and SF (Fig. 9c), although in our case this was the strongest of all PRI:SF relationships ( $r^2=0.79$ ). Unfortunately, the canopy SF of mixed forest stands (e.g., F89, F98) and of more complex canopies is difficult to simulate with 5-Scale and would require more sophisticated modeling approaches (e.g., ray-tracing). It would be worthwhile to eventually obtain estimates of SF for these sites and see if they follow the same trends as the other sites, although this is beyond the scope of the current study.

Hall et al. (in press) and Hilker et al. (2008) conducted an in-depth analysis of the relationships between PRI, LUE and shadow fraction using a sweeping spectroradiometer mounted on a flux tower over a Douglas fir (*Pseudotsuga menziesii* subsp. *menziesii*) forest in coastal British Columbia. They were able to clearly demonstrate the short time response of the sunlit canopy fraction at 531 nm and it correlated well with LUE. They also provide a framework for using multi-angle optical remote sensing for monitoring LUE.

## 5. Conclusions

This study demonstrated a regional-level correlation between clear-sky values of flux tower LUE and different formulations of MODIS PRI when a range of boreal forest cover types and successional stages were analyzed. For all reference bands tested (centered at 488, 551, and 678 nm, respectively), the relationships were stronger when we used MODIS ocean band images acquired closer to the back-scattering direction. Adding a MODIS-derived PRI term to the APAR significantly improved the prediction of GEP for our flux sites. We used PRI with MODIS band 11 (531 nm) and reference band 12 (551 nm) to derive a regional map of LUE. This map showed greater spatial variability than a LUE map created using the MOD17 approach. While our MODIS PRI-derived LUE map is only a snapshot of clear-sky LUE values at a particular point in time, our approach shows that there is significant potential for estimating LUE from space once robust strategies can be developed for interpolating LUE for periods between clear MODIS observations.

We also found positive correlations between MODIS PRI and pixel shadow fraction (SF) and between tower-derived LUE and SF. These findings suggest that differences in the structural properties of the flux sites could explain both the variability in MODIS PRI and tower LUE observed across the sites since greater LUE has been associated with sites having greater leaf area and therefore greater penetration of diffuse light through the canopy. While we have demonstrated that it is possible to use a MODIS PRI to infer the spatial distribution of LUE for a boreal forest landscape, additional observational studies are crucial for identifying a number of remaining issues (e.g., shadow fraction effects on the PRI signal, changes in relative pigment concentrations, morning/afternoon versus midday LUE, PRI in other

biomes, atmospheric correction) before we can operationally produce LUE estimates from satellite platforms. MODIS does not have the optimal combination of bands, spatial resolution, or sensor design for estimating LUE from space. Improved designs of future satellites could help us build on the current proof of concept to permit more robust modeling of the terrestrial carbon cycle using remote sensing. In the meantime, our approach could be used to determine the feasibility of adjusting MODIS GPP parameters when PRI-determined LUE values were available.

## Acknowledgments

The NASA/GSFC contribution to this study was supported by an award to E. Middleton through the NASA Carbon Cycle Science Program. The Natural Sciences and Engineering Research Council of Canada (NSERC) provided for a Ph.D. fellowship to G. Drolet. We acknowledge support provided to FCRN and BERMS by Canadian funding sources (NSERC, Canadian Foundation for Climate and Atmospheric Sciences, BIOCAP, Canadian Forest Service, Meteorological Service of Canada, Action Plan 2000, PERD, NSERC Discovery Grant to H. Margolis). We thank Louis Gonzalez and Nazmi Saleous for their support with HDFLook and the 6 S model, respectively. We are grateful to Maosheng Zhao for access to the MODIS climatological data and interpolation code that allowed us to utilize these datasets, to scientists at GMAO, especially Mahendra K. Karki, for providing GEOS-4 GMAO data, and to Nicholas Coops and Thomas Hilker for providing some pertinent data about our sites. We acknowledge Sylvain Leblanc for his help on operating the 5-Scale model, and Laura Chasmer for her measurements made at the jack pine sites. We thank Robert Knox for his useful inputs along the way. H. Margolis gratefully acknowledges sabbatical and visiting scientist support from the GEST Center of the University of Maryland, Baltimore County, Caelum Research, and the NASA Terrestrial Ecology Program.

## References

- Ahl, D. E., Gower, S. T., Mackay, D. S., Burrows, S. N., Norman, J. M., & Diak, G. R. (2004). Heterogeneity of light use efficiency in a northern Wisconsin forest: Implications for modeling net primary production with remote sensing. *Remote Sensing of Environment*, 93, 168–178.
- Amiro, B. D., Barr, A. G., Black, T. A., Iwashita, H., Kljun, N., McCaughey, J. H., et al. (2006). Carbon, energy and water fluxes at mature and disturbed forest sites, Saskatchewan, Canada. *Agricultural and Forest Meteorology*, 136, 237–251.
- Baldocchi, D. D., & Vogel, C. A. (1996). Energy and CO<sub>2</sub> flux densities above and below a temperate broad-leaved forest and a boreal pine forest. *Tree Physiology*, 16, 5–16.
- Baldocchi, D. D., Vogel, C. A., & Hall, B. (1997). Seasonal variation of carbon dioxide exchange rates above and below a boreal jack pine forest. *Agricultural and Forest Meteorology*, 83, 147–170.
- Barbieri, R., Montgomery, H., Qiu, S., Barnes, B., Knowles, D., Jr., Che, N., et al. (1997). *The MODIS Level 1B Algorithm Theoretical Basis Document Version 2.0 (ATBMOD-01)*. Greenbelt, Maryland 20771, USA: NASA Goddard Space Flight Center (68 pp).
- Barr, A. G., Black, T. A., Hogg, E. H., Griffis, T. J., Morgenstern, K., Kljun, N., et al. (2007). Climatic controls on the carbon and water balances of a boreal aspen forest, 1994–2003. *Global Change Biology*, 13, 561–576.
- Barr, A. G., Black, T. A., Hogg, E. H., Kljun, N., Morgenstern, K., & Nesic, Z. (2004). Inter-annual variability in the leaf area index of a boreal aspen–hazelnut forest in relation to net ecosystem production. *Agricultural and Forest Meteorology*, 126, 237–255.
- Barton, C. V. M., & North, P. R. J. (2001). Remote sensing of canopy light use efficiency using the photochemical reflectance index – Model and sensitivity analysis. *Remote Sensing of Environment*, 78, 264–273.
- Bilger, W., & Björkman, O. (1990). Role of the xanthophyll cycle in photoprotection elucidated by measurements of light-induced absorbance changes, fluorescence and photosynthesis in leaves of *Hedera canariensis*. *Photosynthesis Research*, 25, 173–185.
- Black, T. A., DenHartog, G., Neumann, H. H., Blanken, P. D., Yang, P. C., Russell, C., et al. (1996). Annual cycles of water vapour and carbon dioxide fluxes in and above a boreal aspen forest. *Global Change Biology*, 2, 219–229.
- Chen, J. M. (1996). Canopy architecture and remote sensing of the fraction of photosynthetically active radiation absorbed by boreal conifer forests. *IEEE Transactions on Geoscience and Remote Sensing*, 34(6), 1353–1368.
- Chen, J. M., Govind, A., Sonnentag, O., Zhang, Y. Q., Barr, A., & Amiro, B. (2006). Leaf area index measurements at Fluxnet-Canada forest sites. *Agricultural and Forest Meteorology*, 140, 257–268.
- Cheng, Y. F., Gamon, J. A., Fuentes, D. A., Mao, Z. Y., Sims, D. A., Qiu, H. L., et al. (2006). A multi-scale analysis of dynamic optical signals in a Southern California chaparral

- ecosystem: A comparison of field, AVIRIS and MODIS data. *Remote Sensing of Environment*, 103, 369–378.
- Ciais, P., Reichstein, M., Viovy, N., Granier, A., Ogee, J., Allard, V., et al. (2005). Europe-wide reduction in primary productivity caused by the heat and drought in 2003. *Nature*, 437, 529–533.
- Coursolle, C., Margolis, H. A., Barr, A. G., Black, T. A., Amiro, B. D., McCaughey, J. H., et al. (2006). Late-summer carbon fluxes from Canadian forests and peatlands along an east-west continental transect. *Canadian Journal of Forest Research*, 36, 783–800.
- Demmig-Adams, B. (2003). Linking the xanthophyll cycle with thermal energy dissipation. *Photosynthesis Research*, 76, 73–80.
- Drolet, G. G., Huemmrich, K. F., Hall, F. G., Middleton, E. M., Black, T. A., Barr, A. G., et al. (2005). A MODIS-derived photochemical reflectance index to detect inter-annual variations in the photosynthetic light-use efficiency of a boreal deciduous forest. *Remote Sensing of Environment*, 98, 212–224.
- Fensholt, R., Sandholt, I., & Rasmussen, M. S. (2004). Evaluation of MODIS LAI,  $f_{APAR}$  and the relation between  $f_{APAR}$  and NDVI in a semi-arid environment using in situ measurements. *Remote Sensing of Environment*, 91, 490–507.
- Filella, I., Amaro, T., Araus, J. L., & Penuelas, J. (1996). Relationship between photosynthetic radiation-use efficiency of Barley canopies and the photochemical reflectance index (PRI). *Physiologia Plantarum*, 96, 211–216.
- Fuentes, D. A., Gamon, J. A., Cheng, Y. F., Claudio, H. C., Qiu, H. L., Mao, Z. Y., et al. (2006). Mapping carbon and water vapor fluxes in a chaparral ecosystem using vegetation indices derived from AVIRIS. *Remote Sensing of Environment*, 103, 312–323.
- Gamon, J. A., Field, C. B., Bilger, W., Björkman, O., Fredeen, A. L., & Penuelas, J. (1990). Remote sensing of the xanthophyll cycle and chlorophyll fluorescence in sunflower leaves and canopies. *Oecologia*, 85, 1–7.
- Gamon, J. A., Penuelas, J., & Field, C. B. (1992). A narrow-waveband spectral index that tracks diurnal changes in photosynthetic efficiency. *Remote Sensing of Environment*, 41, 35–44.
- Gamon, J. A., Serrano, L., & Surfus, J. S. (1997). The photochemical reflectance index: An optical indicator of photosynthetic radiation use efficiency across species, functional types, and nutrient levels. *Oecologia*, 112, 492–501.
- Goulden, M. L., Munger, J. W., Fan, S. M., Daube, B. C., & Wofsy, S. C. (1996). Measurements of carbon sequestration by long-term eddy covariance: Methods and a critical evaluation of accuracy. *Global Change Biology*, 2, 169–182.
- Gower, S. T., Kucharik, C. J., & Norman, J. M. (1999). Direct and indirect estimation of leaf area index,  $f_{APAR}$ , and net primary production of terrestrial ecosystems. *Remote Sensing of Environment*, 70, 29–51.
- Grace, J., Nichol, C., Disney, M., Lewis, P., Quaife, T., & Bowyer, P. (2007). Can we measure terrestrial photosynthesis from space directly, using spectral reflectance and fluorescence? *Global Change Biology*, 13, 1484–1497.
- Grant, R. F., & Nalder, I. A. (2000). Climate change effects on net carbon exchange of a boreal aspen-hazelnut forest: Estimates from the ecosystem model ecosys. *Global Change Biology*, 6, 183–200.
- Gu, L. H., Baldocchi, D., Verma, S. B., Black, T. A., Vesala, T., Falge, E. M., et al. (2002). Advantages of diffuse radiation for terrestrial ecosystem productivity. *Journal of Geophysical Research-Atmospheres*, 107, D6. doi:10.1029/2001JD001042.
- Hall, F. G., Hilker, T., Coops, N. C., Lyapustin, A., Huemmrich, K. F., Middleton, E. M., in press. Multi-angle remote sensing of forest light use efficiency by observing PRI variation with canopy shadow fraction. *Remote Sensing of Environment*.
- Hall, F. G., Shimabukuro, Y. E., & Huemmrich, K. F. (1995). Remote sensing of forest biophysical structure using mixture decomposition and geometric reflectance models. *Ecological Applications*, 5, 993–1013.
- Heijmans, M. M. P. D., Arp, W. T., & Chapin, F. S. (2004). Carbon dioxide and water vapour exchange from understory species in boreal forest. *Agricultural and Forest Meteorology*, 123, 135–147.
- Heinsch, F. A., Reeves, M., Bowker, C. F., Votava, P., Kang, S., Milesi, C., et al. (2003). *User's Guide: GPP and NPP (MOD17A2/A3) products. NASA MODIS Land Algorithm. Version 2.0.* <http://www.nts.gov/umt/modis/MOD17UsersGuide.pdf>
- Heinsch, F. A., Zhao, M., Running, S. W., Kimball, J. S., Nemani, R. R., Davis, K. J., et al. (2006). Evaluation of remote sensing based terrestrial productivity from MODIS using regional tower eddy flux network observations. *IEEE Transactions on Geoscience and Remote Sensing*, 44(7), 1908–1925.
- Hilker, T., Coops, N. C., Hall, F. G., Black, T. A., Wulder, M. A., & Nesic, Z. (2008). Separating physiologically and directionally induced changes in PRI using BRDF models. *Remote Sensing of Environment*, 112, 2777–2788 (Available online March 10, 2008).
- Hill, M. J., Held, A. A., Leuning, R., Coops, N. C., Hughes, D., & Cleugh, H. A. (2006). MODIS spectral signals at a flux tower site: Relationships with high-resolution data, and CO<sub>2</sub> flux and light use efficiency measurements. *Remote Sensing of Environment*, 103, 351–368.
- Hollinger, D. Y., Kelliher, F. M., Byers, J. N., Hunt, J. E., McSeveny, T. M., & Weir, P. L. (1994). Carbon dioxide exchange between an undisturbed old-growth temperate forest and the atmosphere. *Ecology*, 75, 134–150.
- Jarvis, P. G., Massheder, J. M., Hale, S. E., Moncrieff, J. B., Rayment, M., & Scott, S. L. (1997). Seasonal variation of carbon dioxide, water vapor, and energy exchanges of a boreal black spruce forest. *Journal of Geophysical Research-Atmospheres*, 102, 28953–28966.
- Jenkins, J. P., Richardson, A. D., Braswell, B. H., Ollinger, S. V., Hollinger, D. Y., & Smith, M. L. (2007). Refining light-use efficiency calculations for a deciduous forest canopy using simultaneous tower-based carbon flux and radiometric measurements. *Agricultural and Forest Meteorology*, 143, 64–79.
- Kolari, P., Pumpanen, J., Kulmala, L., Ilvesniemi, H., Nikinmaa, E., Gronholm, T., & Hari, P. (2006). Forest floor vegetation plays an important role in photosynthetic production of boreal forests. *Forest Ecology and Management*, 221, 241–248.
- Landsberg, J. J., & Waring, R. H. (1997). A generalised model of forest productivity using simplified concepts of radiation-use efficiency, carbon balance and partitioning. *Forest Ecology and Management*, 95, 209–228.
- Leblanc, S. G., & Chen, J. M. (2000). A Windows Graphic User Interface (GUI) for the Five-Scale model for fast BRDF simulations. *Remote Sensing Reviews*, 19, 293–305.
- Liu, J., Chen, J. M., Cihlar, J., & Park, W. M. (1997). A process-based boreal ecosystem productivity simulator using remote sensing inputs. *Remote Sensing of Environment*, 62, 158–175.
- Lotsch, A., Tian, Y., Friedl, M. A., & Myneni, R. B. (2003). Land cover mapping in support of LAI and FPAR retrievals from EOS-MODIS and MISR: Classification methods and sensitivities to errors. *International Journal of Remote Sensing*, 24(10), 1997–2016.
- Margolis, H. A., Flanagan, L. B., & Amiro, B. D. (2006). The Fluxnet-Canada Research Network: Influence of climate and disturbance on carbon cycling in forests and peatlands. *Agricultural and Forest Meteorology*, 140, 1–5.
- Martel, M. C., Margolis, H. A., Coursolle, C., Bigras, F. J., Heinsch, F. A., & Running, S. W. (2005). Decreasing photosynthesis at different spatial scales during the late growing season on a boreal cutover. *Tree Physiology*, 25, 689–699.
- McMurtrie, R. E., Rook, D. A., & Kelliher, F. M. (1990). Modelling the yield of *Pinus radiata* on a site limited by water and nitrogen. *Forest Ecology and Management*, 30, 381–413.
- Monteith, J. L. (1972). Solar-radiation and productivity in tropical ecosystems. *Journal of Applied Ecology*, 9, 747–766.
- Morén, A. S., & Lindroth, A. (2000). CO<sub>2</sub> exchange at the floor of a boreal forest. *Agricultural and Forest Meteorology*, 101, 1–14.
- Myneni, R. B., Nemani, R. R., & Running, S. W. (1997). Estimation of global leaf area index and absorbed PAR using radiative transfer models. *IEEE Transactions on Geoscience and Remote Sensing*, 35(6), 1380–1393.
- Ni, W. G., Li, X. W., Woodcock, C. E., Roujean, J. L., & Davis, R. E. (1997). Transmission of solar radiation in boreal conifer forests: Measurements and models. *Journal of Geophysical Research-Atmospheres*, 102, 29555–29566.
- Nichol, C. J., Huemmrich, K. F., Black, T. A., Jarvis, P. G., Walthall, C. L., Grace, J., et al. (2000). Remote sensing of photosynthetic-light-use efficiency of boreal forest. *Agricultural and Forest Meteorology*, 101, 131–142.
- Nouvellon, Y., Seen, D. L., Rambal, S., Begue, A., Moran, M. S., Kerr, Y., et al. (2000). Time course of radiation use efficiency in a shortgrass ecosystem: Consequences for remotely sensed estimation of primary production. *Remote Sensing of Environment*, 71, 43–55.
- Peddle, D. R., Hall, F. G., & LeDrew, E. F. (1999). Spectral mixture analysis and geometric-optical reflectance modeling of boreal forest biophysical structure. *Remote Sensing of Environment*, 67, 288–297.
- Penuelas, J., Filella, I., & Gamon, J. A. (1995). Assessment of photosynthetic radiation-use efficiency with spectral reflectance. *New Phytologist*, 131, 291–296.
- Potter, C. S., Randerson, J. T., Field, C. B., Matson, P. A., Vitousek, P. M., Mooney, H. A., et al. (1993). Terrestrial ecosystem production: A process model based on global satellite and surface data. *Global Biogeochemical Cycles*, 7, 811–841.
- Prince, S. D., & Goward, S. N. (1995). Global primary production: A remote sensing approach. *Journal of Biogeography*, 22, 815–835.
- Rahman, A. F., Cordova, V. D., Gamon, J. A., Schmid, H. P., & Sims, D. A. (2004). Potential of MODIS ocean bands for estimating CO<sub>2</sub> flux from terrestrial vegetation: A novel approach. *Geophysical Research Letters*, 31, L10503. doi:10.1029/2004GL019778.
- Rahman, A. F., Gamon, J. A., Fuentes, D. A., Roberts, D. A., & Prentiss, D. (2001). Modeling spatially distributed ecosystem flux of boreal forest using hyperspectral indices from AVIRIS imagery. *Journal of Geophysical Research-Atmospheres*, 106, 33579–33591.
- Ruimy, A., Saugier, B., & Dedieu, G. (1994). Methodology for the estimation of net primary production from remotely sensed data. *Journal of Geophysical Research-Atmospheres*, 99, 5263–5283.
- Running, S. W., Baldocchi, D. D., Turner, D. P., Gower, S. T., Bakwin, P. S., & Hibbard, K. A. (1999). A global terrestrial monitoring network integrating tower fluxes, flask sampling, ecosystem modeling and EOS satellite data. *Remote Sensing of Environment*, 70, 108–127.
- Running, S. W., Nemani, R. R., Heinsch, F. A., Zhao, M. S., Reeves, M., & Hashimoto, H. (2004). A continuous satellite-derived measure of global terrestrial primary production. *Bioscience*, 54, 547–560.
- Running, S. W., Nemani, R. R., Peterson, D. L., Band, L. E., Potts, D. F., Pierce, L. L., et al. (1989). Mapping regional forest evapotranspiration and photosynthesis by coupling satellite data with ecosystem simulation. *Ecology*, 70, 1090–1101.
- SAS Institute (2000). *SAS/STAT user's guide, vol. 1* (4th ed.). Cary, SC, USA: SAS Institute.
- Schwalm, C. R., Black, T. A., Amiro, B. D., Arain, M. A., Barr, A. G., Bourque, C. P. A., et al. (2006). Photosynthetic light use efficiency of three biomes across an east-west continental-scale transect in Canada. *Agricultural and Forest Meteorology*, 140, 269–286.
- Serrano, L., & Penuelas, J. (2005). Assessing forest structure and function from spectral transmittance measurements: A case study in a Mediterranean holm oak forest. *Tree Physiology*, 25, 67–74.
- Sims, D. A., Luo, H. Y., Hastings, S., Oechel, W. C., Rahman, A. F., & Gamon, J. A. (2006). Parallel adjustments in vegetation greenness and ecosystem CO<sub>2</sub> exchange in response to drought in a Southern California chaparral ecosystem. *Remote Sensing of Environment*, 103, 289–303.
- Sims, D. A., Rahman, A. F., Cordova, V. D., Baldocchi, D. D., Flanagan, L. B., Goldstein, A. H., et al. (2005). Midday values of gross CO<sub>2</sub> flux and light use efficiency during satellite overpasses can be used to directly estimate eight-day mean flux. *Agricultural and Forest Meteorology*, 131, 1–12.
- SPSS (2002). *SigmaPlot 8.0 User's Guide*. Chicago, IL, USA: SPSS Inc.
- Steinberg, D. C., Goetz, S. J., & Hyer, E. J. (2006). Validation of MODIS FPAR products in boreal forests of Alaska. *IEEE Transactions on Geoscience and Remote Sensing*, 44, 1818–1828.
- Stylinski, C. D., Gamon, J. A., & Oechel, W. C. (2002). Seasonal patterns of reflectance indices, carotenoid pigments and photosynthesis of evergreen chaparral species. *Oecologia*, 131, 366–374.



- Trotter, C. M., Leathwick, J. R., & Pairman, D. (2001). Spatial information for ecosystem classification, analysis, and forecasting. In P. J. Halls (Ed.), *Spatial Information and the Environment* (pp. 7–36). New York: Taylor and Francis.
- Trotter, G. M., Whitehead, D., & Pinkney, E. J. (2002). The photochemical reflectance index as a measure of photosynthetic light use efficiency for plants with varying foliar nitrogen contents. *International Journal of Remote Sensing*, 23, 1207–1212.
- Turner, D. P., Guzy, M., Lefsky, M. A., Ritts, W. D., Van Tuyl, S., & Law, B. E. (2004). Monitoring forest carbon sequestration with remote sensing and carbon cycle modeling. *Environmental Management*, 33, 457–466.
- Turner, D. P., Ollinger, S. V., & Kimball, J. S. (2004). Integrating remote sensing and ecosystem process models for landscape- to regional-scale analysis of the carbon cycle. *Bioscience*, 54, 573–584.
- Turner, D. P., Ritts, W. D., Cohen, W. B., Maeirsperger, T. K., Gower, S. T., Kirschbaum, A. A., et al. (2005). Site-level evaluation of satellite-based global terrestrial gross primary production and net primary production monitoring. *Global Change Biology*, 11, 666–684.
- Turner, D. P., Urbanski, S., Bremer, D., Wofsy, S. C., Meyers, T., Gower, S. T., et al. (2003). A cross-biome comparison of daily light use efficiency for gross primary production. *Global Change Biology*, 9, 383–395.
- Vermote, E. F., Tanre, D., Deuzé, J. L., Herman, M., & Morcrette, J. J. (1997). Second Simulation of the Satellite Signal in the Solar Spectrum, 6 S: An overview. *IEEE Transactions on Geoscience and Remote Sensing*, 35, 675–686.
- Whitehead, D., & Gower, S. T. (2001). Photosynthesis and light-use efficiency by plants in a Canadian boreal forest ecosystem. *Tree Physiology*, 21, 925–929.
- Wofsy, S. C., Goulden, M. L., Munger, J. W., Fan, S. M., Bakwin, P. S., Daube, B. C., et al. (1993). Net exchange of CO<sub>2</sub> in a midlatitude forest. *Science*, 260, 1314–1317.
- Xiong, X., Sun, J., Barnes, W., Salomonson, V., Esposito, J., Erives, H., & Guenther, B. (2007). Multiyear On-Orbit Calibration and Performance of Terra MODIS Reflective Solar Bands. *IEEE Transactions on Geoscience and Remote Sensing*, 45(4), 879–889.
- Yamamoto, H. Y. (1979). Biochemistry of the violaxanthin cycle in higher plants. *Pure and Applied Chemistry*, 51, 639–648.
- Yang, W., Huang, D., Tan, B., Stroeve, J. C., Shabanov, N. V., Knyazikhin, Y., Nemani, R. R., & Myneni, R. B. (2006). Analysis of leaf area index and fraction of PAR absorbed by vegetation products from the Terra MODIS sensor: 2000–2005. *IEEE Transactions on Geoscience and Remote Sensing*, 44(7), 1829–1842.
- Zhao, M. S., Heinsch, F. A., Nemani, R. R., & Running, S. W. (2005). Improvements of the MODIS terrestrial gross and net primary production global data set. *Remote Sensing of Environment*, 95, 164–176.